PARP1 and PARylation facilitate transcription-coupled DNA repair by stabilizing the CSB-RNAPII complex

Robu, M.; Shah, R.G.; Heuvel, D. van den; Coulombe, Y.; Bazin, M.; Woude, M. van der; ... ; Shah, G.M.

Nucleic Acids Research, 2025, **53**, gkaf1303
https://doi.org/10.1093/nar/gkaf1303
Genome integrity, repair and replication

PARP1 and PARylation facilitate transcription-coupled DNA repair by stabilizing the CSB–RNAPII complex

Mihaela Robu[1], Rashmi G. Shah[1], Diana van den Heuvel[2], Yan Coulombe[3], Marc Bazin[1], Melanie van der Woude[4], Angela Kragten[2], Hannes Lans[4], John M. Pascal[5], Jean-Yves Masson[3,6], Martijn S. Luijsterburg[2], Girish M. Shah[1,6,*]

[1]CHU de Quebec Laval University Research Centre, Neuroscience Axis, Quebec City (QC), G1V 4G2, Canada
[2]Leiden University Medical Centre, Leiden, 233ZG, the Netherlands
[3]CHU de Quebec Laval University Research Centre, Oncology Axis, G1J 1Z4, Canada
[4]Erasmus University Medical Center, Erasmus MC Cancer Institute, Rotterdam, 1355, the Netherlands
[5]Université de Montreal,, Montreal, H3T 1J4, Canada
[6]Department of Molecular Biology, Medical Biochemistry and Pathology, Faculty of Medicine, and Cancer Research Centre of Laval University Quebec City, QC, G1V 0A6, Canada

*To whom correspondence should be addressed. girish.shah@crchudequebec.ulaval.ca

Abstract

Transcription-coupled nucleotide excision repair (TC-NER or TCR) is initiated when the ATPase Cockayne syndrome protein B (CSB) recognizes a DNA lesion stalled RNA polymerase II (RNAPII) and forms a stable complex. Here, we report that poly(ADP-ribose) polymerase-1 (PARP1), that plays a key role in the lesion recognition step of global genomic NER, also facilitates the earliest step of TCR. PARP1, which is associated with RNAPII during normal transcription, interacts with and stabilizes CSB on the lesion-stalled RNAPII. CSB stimulates PARP1's activity to form PAR, and in turn CSB is PARylated mainly at its N-terminal PAR-binding motif (PBM) to promote its stabilization with RNAPII, whereas its minor PARylation at the C-terminal domain suppresses its ATPase function, thus limiting the window of time for ATP-dependent lesion recognition by CSB. The loss of PARP1, treatment with inhibitors of PARP or poly(ADP-ribose) glycohydrolase (PARG) to prevent PAR synthesis or its catabolism to generate free PAR or engineering N-terminal PARylation-resistant CSB decrease the efficiency of cells for TCR. PARP1 mutant *Caenorhabditis elegans* larvae exhibit a pronounced TCR-deficient phenotype. Our findings uncover an evolutionarily conserved role of PARP1 and PAR metabolism in the initiation of TCR.

Graphical abstract

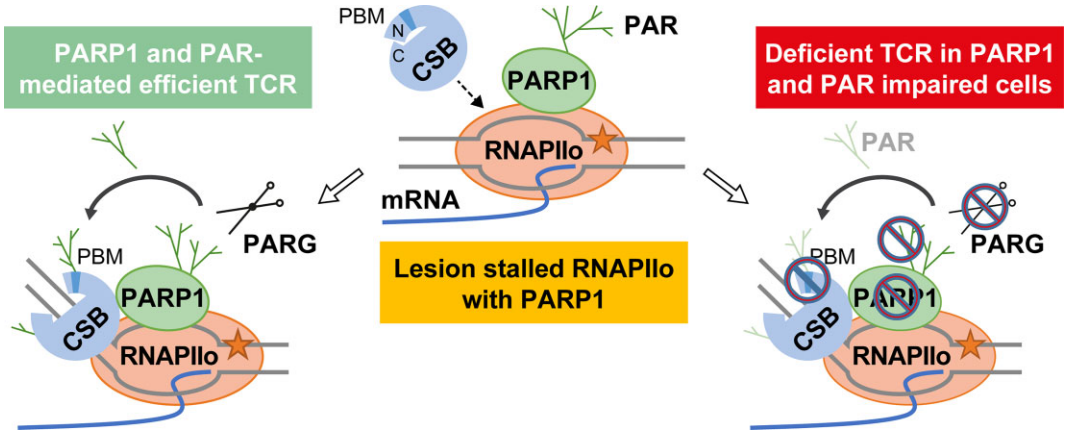

Introduction

The transcription-coupled nucleotide excision repair (TC-NER or TCR) is a sub-pathway of NER that rapidly removes bulky DNA lesions from the transcribed strand of transcriptionally active genes [1–3]. Since such DNA lesions cause a global shut-down of transcription, TCR prioritizes the repair of these lesions to permit resumption of transcription [4]. TCR is activated when the elongating form of RNA polymerase

Received: January 31, 2025. **Revised:** October 22, 2025. **Accepted:** October 23, 2025

II (RNAPII) in the process of transcription stalls at a DNA lesion. The Cockayne syndrome protein B (CSB), an autoinhibitory SWI/SNF-like translocase, which dynamically probes RNAPII during normal transcription, recognizes the lesion-stalled RNAPII and forms a stable complex. After an ATP-dependent lesion recognition process, CSB initiates TCR by recruiting the CSA-DDB1-Cul4A-Rbx1 ($CRL4^{CSA}$) ubiquitin ligase complex that ubiquitinates CSB and RNAPII [5, 6]. The UVSSA-USP7 complex is recruited by CSA to perform multiple functions during TCR. USP7 deubiquitinates CSB, and thus determines the length of CSB stay at the lesion site [7]. UVSSA together with ELOF1 [8, 9] stabilizes the positioning of the CSA-ligase complex on RNAPII, resulting in efficient ubiquitination of RNAPII [10]. The mono-ubiquitination of UVSSA is required for recruitment and transfer of TFIIH to the stalled ubiquitinated RNAPII [5, 6]. The newly identified protein STK19 positions TFIIH on RNAPII and stimulates the removal of poly-ubiquitinated RNAPII [11–14]. Together, the cooperative actions of CSB, CSA, ELOF1, STK19, and UVSSA result in recruitment of the downstream TCR proteins to remove a piece of single-stranded DNA containing the lesion, synthesize a new strand using old undamaged strand as a template, seal the gap and restore the DNA to its native state [15]. While the essential steps of the TCR process are known, there are many gaps in our understanding of this pathway, starting from the mechanism by which CSB recognizes and binds to DNA damage stalled RNAPII [16]. In this context, a number of associated factors are being identified that participate in different steps of TCR resulting in a more efficient repair and/or restart of transcription, such as PAF1 [17], LEO1 [18], FACT subunit Spt16 [19], SMARCA5 [20], NAP1-like histone chaperones [21], and DDA1 [22].

In mammalian cells, poly(ADP-ribose) polymerase-1 (PARP1) is among the earliest proteins that binds to and be activated by a wide variety of DNA lesions [23]. There are three functional domains in PARP1: the N-terminal DNA-binding domain (DBD), the automodification domain, and the C-terminal domain, which includes the WGR domain and the catalytic domain (CAT) responsible for enzyme activity [24]. The activated PARP1 utilizes NAD^+ to make polymers of ADP-ribose (PAR) which post-translationally modify or PARylate PARP1 and other PAR-accepting target proteins in the vicinity of DNA damage [25]. These PARylated proteins transiently acquire new functions, such as an altered affinity for DNA and other protein partners, or susceptibility to other post-translational modifications (PTM) [26, 27]. Several PAR-binding domains have been identified, including the high affinity PAR-binding motif (PBM), a 20 aa conserved sequence containing a cluster rich in hydrophobic and basic residues [28–30]. Finally, poly(ADP-ribose) glycohydrolase (PARG), rapidly digests PAR chains by exo- and endo-glycohydrolase activities [31, 32] to liberate mono-ADP-ribose units as well as fragments of PAR chains that noncovalently PARylate additional PAR-acceptor proteins to alter their functions. This rapid, cascading and reversible PARylation, confers distinct mechanistic roles to different DNA repair pathways through its association with different PAR acceptor partner proteins [33–36].

PARP1 and PARylation have previously been shown by us and others [37–39] to increase the efficiency of the global genome sub-pathway of NER (GGR) that repairs the majority of the genomic lesions. At the ultraviolet (UV)-lesion site, PARP1 interacts with the early lesion binding protein DDB2 which in turn stimulates its catalytic activity, resulting in PARylation of both DDB2 and DDB1 to promote downstream GGR events [40–42]. Furthermore, PARP1 interacts with XPC in the nucleoplasm and escorts it to the damage site on chromatin [43]. Lastly, XPC stimulates the catalytic activity of PARP1 resulting in recruitment of the PAR-regulated chromatin remodeler ALC1 which facilitates GGR [44]. Moreover, PARP1 and PARylation play different roles in normal transcription [45], such as compete with and replace histone H1 at the promoter site of many actively transcribed genes [46], displace core histones from nucleosome to facilitate *in vitro* transcription by RNAPII [47] and PARylate the negative elongation factor NELF to transition from the promoter-paused into the elongation phase of transcription [48].

In view of these roles of PARP1 and PARylation in GGR and normal transcription, we examined whether PARP1 also plays a role in TCR, which was indicated in previous studies. PARP-inhibitor (PARPi) was shown to delay repair of UV lesions in normal cells but not in CS-B cells [49] and PARP1-knockdown (PARP1-kd) was reported by us to suppresses repair of UV-damaged viral reporter genes in GGR-deficient XP-C cells [50]. Hence, PARP1 and CSB, which are already collaborating for the removal of a variety of DNA lesions [51] could also be cooperating in TCR. In a genome-wide CRISPR-Cas9 screens, PARP1 was identified as one of the hits sensitizing the cells to transcription-blocking lesions [52]. Here, we report a direct role of PARP1 and PARylation in promoting the key interaction of CSB with the lesion-stalled RNAPII that leads to the launch of TCR.

Materials and methods

Cell lines, clones, and transient transfection

Parental SV-40–immortalized GM637, CS-B (GM16095, TCR deficient) and XP-C (GM15983, GGR deficient) human skin fibroblasts were obtained from Coriell and HEK293 and U2OS cells from ATCC. The creation of the clones PARP1-replete GMU6 and XPCU6, PARP1-depleted GMshPARP1 and XPCshPARP1, the Bio-ID PARP1 clones [41, 53], following U2OS clones, namely PARP1-ko [44], CSB-ko, CSA-ko, and doxycycline-inducible GFP-CSB [54] have all been described. To generate knockout cell lines, GM637 were either transfected with pSpCas9 (BB) 2A puro (pX459, Addgene, 62988) containing the single guide RNA (sgRNA) targeting PARP1 (5'-CACCGAAGGTGGGCCACTCCATC-3') or co-transfected with Cas9-2A-GFP (pX458, Addgene, 48138) and pLV-U6g-PPB (Sigma–Aldrich) encoding a sgRNA for CSB, as described [54]. For expression of GFP-PARP1, GFP-CSB or their fragments, HEK293 PARP1-ko or HEK293 parental cells were transiently transfected with HEBS-CaCl2 and 48 h after the cells were collected for immunoprecipitation (IP) studies.

To generate doxycycline-inducible CSB PAR resistant (PARr-CSB) cell lines, U2OS CSB-ko cells were transfected with pcDNA5/FRT/TO/puro vector encoding the respective gene-of-interest. Transfected cells were selected on puromycin (1 μg/ml) for 3 days and plated at low density. Individual clones were verified for the knockout efficiency and CSB expression induced with 1 mg/ml doxycycline for 24 h by western blot. For UDS-TCR studies, XPC was knocked down in the wt-CSB and PARr-CSB U2OS cells, as de-

scribed [55] using the short hairpin RNA (shRNA) for XPC cloned in pLKO.1-puro vector targeting XPC mRNA sequences 5′-CCCACTGCCATTGGCTTATAT-3′ (clone number TRCN0000083119) that was retrieved from the Sigma Mission TRC human 1.5 shRNA library (gift from Stéphane Gobeil, CHU de Québec Laval University Research Center).

Plasmids and cloning

The GFP-PARP1 vector and GFP-PARP1 E988A [56] were made resistant to RNAi by site directed mutagenesis as previously described [57]. To create the GFP-PARP1 BRCT-CAT, the PARP1 cDNA FLAG-hPARP1-RSiP-CMV 7.1 plasmid [41] was digested with EcoRI and the 2074 bp EcoRI/EcoRI fragment was blunt ligated into GFP-C1 plasmid digested with EcoRI/EcoICRI after modification of the DNA ends by Klenow enzyme. The CAT domain was made by digesting the above BRCT-CAT cDNA with PvuII and ligation of the 1492 bp fragment into EcoRI/EcoICRI fragment of GFP-C1 plasmid. To create BRCT domain, the BRCT-CAT was digested and the 5276 kb fragment was purified from the agarose gel and religated. Plasmid transfection was performed using TurboFect reagent according to the manufacturer's protocol (Thermo Fisher Scientific). The GFP-CSB-wt and its fragments were described [8]. The PAR resistant CSB mutant was generated by site-directed mutagenesis PCR, as previously described [58].

Chemicals and antibodies

In the indicated experiments, the following compounds were used: 2 μM PARPi olaparib (LC Laboratories), 100 nM BMN637 (Cayman Chemical), 2 μM PARPi ABT-888 (Santa Cruz Biotechnology), 1 μM PARG inhibitor (PDD 00017273 Tocris), Illudin S (Cayman Chemical), 100 μM 5,6-dichlorobenzimidazole 1β D-ribofuranoside (DRB) from Sigma–Aldrich, 500 nM flavopiridol hydrochloride (Sigma–Aldrich). Antibodies are listed in Supplementary Table S1.

Cell fractionation and co-IP of proteins in the cell fractions

Cell fractionation to obtain nucleoplasm and chromatin extract and the co-IP studies were done as described [41]. Where indicated, DNA damage was induced by UVC (30 J/m2) or Illudin S (30 ng/ml) and the catalytic activity of PARP1 or PARG was inhibited by addition of PARPi or PARGi for 15 min or 1 h, respectively, prior to treatment of cells. The protein content in each fraction was estimated by Bradford assay and an equal amount of protein from each sample was subjected to co-IP studies. For the streptavidin–IP, 50 μM biotin was added in the medium 16–18 h before UV-treatment and Bio-ID PARP1 cell fractionation, followed by IP with M280 streptavidin beads for 30 min at ambient temperature. The beads were washed as suggested in the supplier's manual (Life Technologies). For RNAPIIS2 IP to study the downstream proteins, the cells were lysed in IP-130 buffer [30 mM Tris (pH 7.5), 130 mM NaCl, 2 mM $MgCl_2$, 0.5% Triton X-100, protease inhibitor cocktail (Roche)] for 20 min on ice followed by centrifugation and removal of the supernatant. The pellet was suspended in IP-buffer with 50 U/ml Benzonase® (Sigma–Aldrich) and incubated at room temperature (RT) for 30 min while rotating. An equal amount of protein as estimated by Bradford was subjected to IP with 2 μg RNAPIIS2 (ab5095, Abcam) for 2–3 h at 4°C. Protein complexes were recovered by incubation with Dynabeads protein G magnetic beads (Invitrogen) for 1 h at 4°C.

U2OS GFP-CSB cells were mock treated or irradiated with UVC light (20 J/m^2) and harvested 1 h after UV. For the immunoprecipitation of GFP-tagged proteins, the cell pellets were solubilized in EBC-150 buffer [50 mM Tris (pH 7.5), 150 mM NaCl, 2 mM $MgCl_2$, 0.5% NP-40, and protease inhibitor cocktail (Roche, 11836170001)] supplemented with 500 U Benzonase, without chromatin fractionation, and pull-down was performed using GFP Trap beads (Chromotek). After incubation, the beads were washed six times with EBC-2 (300) buffer [50 mM Tris (pH 7.5), 300 mM NaCl, 1 mM ethylenediaminetetraacetic acid (EDTA), 0.5% NP-40, and protease inhibitor cocktail (Roche)]. After final washes, beads were resuspended in 20 μl Laemmli–sodium dodecyl sulphate (SDS) sample buffer. For subsequent analysis by western blotting, the samples were boiled for 10 min at 95°C.

UV irradiation and immunofluorescence microscopy studies

Cells were grown on circular 12 mm coverslips in 24-well cluster to 80% confluence. When indicated, the transcription inhibitors DRB or flavopiridol, and the PARPi or PARGi were added in the media 1 h before UVC irradiation of the cells. For **Recovery of RNA synthesis (RRS) studies,** global-UVC irradiated (10 J/m^2) or Illudin S treated (30 ng/ml for 3 h) cells were allowed to recover for the indicated time points and pulse-labelled 1 h before fixation with 1 mM 5-EU (US Biological). Nascent RNA was visualized using Click-iT RNA with either Alexa Fluor 488 or 594 imaging kit according to the manufacturer's protocol (Invitrogen). For **Unscheduled DNA synthesis** (UDS)-TCR, the XP-C cells or shXPC U2Os wt and PARr-CSB were locally irradiated with 100 J/m^2 though a 5 μm polycarbonate filter (Millipore) and immediately pulse-labelled with 10 μM ethynyl deoxyuridine (EdU; Abcam) for 3 or 6 h followed by cells fixation and Click-iT chemistry according to the manufacturer's instructions (Invitrogen). After coupling, the DNA was denatured with 2 N HCl for 5 min at 37C, followed by blocking with 5% bovine serum albumin (BSA; Sigma–Aldrich) in phosphate buffered saline (PBS)–0.1% triton for 30 min. Next, the coverslips were incubated for 2 h at RT with an antibody against cyclobutane primidine dimers (CPD), followed by incubation for 30 min with Alexa488 or 594 conjugated antimouse antibody. The coverslips were mounted in Prolong gold antifade mounting media (Invitrogen). Images of immunostained cells were taken with Zeiss Axiovert 200 at 40× or 63× using the AxioCam MRm.

Clonogenic survival assays

Cells were seeded in triplicate in a six-well cluster at 250 cell per well. The next day, cells were mock treated or exposed to a dilution series of Illudin S for 24 h. The cells were grown for 7 or 14 days before fixation with Coomassie blue. Colonies numbers were counted using GeneTools (Syngene).

UV sensitivity assays in *Caenorhabditis elegans*

UV survival experiments in *C. elegans* were performed as described previously [59]. The wild type strain was Bristol N2 and the mutant alleles were *xpc-1(tm3886)*, *csb-1(ok2335)*, and *PARP1 (ok988)*. The L1 larvae were seeded in quintuple for each UV-B dose (and control) on 6 cm HT115 plates and

irradiated at the indicated UV-B dose using two Philips TL-12 UVB tubes (40 W). The surviving animals that developed 48 h after UV irradiation beyond the L2 stage and the arrested animals as L1/L2 larvae were counted. The survival factor was calculated by dividing the numbers of arrested L1/2 larvae by the number of all larval stages and adult worms. The data were expressed as mean ± standard error of the mean (SEM) from three independent experiments.

Identification of Bio-ID PARP1 interactome by mass spectrometry

The Bio-ID PARP1 cells were fractionated to obtain nucleoplasmic and chromatin-bound protein fraction as described [43]. The streptavidin IP of the chromatin fraction was carried out for 30 min at RT. The beads (Life Technologies) were extensively washed and suspended in 2× volume of Tris-bufferred saline (TBS) containing 30% glycerol and protease inhibitors and stored at −30°C. The PARP1 interacting proteins were identified using Liquid chromatography tandem Mass-spectrometry (LC-MS/MS) and quantified on Dionex Ultimate 3000 nano high performance liquid chromatography (HPLC) system as previously described [60]. Data acquisition was done using Xcalibur version 2.2 SP1.48. Protein identification and quantification was performed using the MaxQuant software package version 1.5.2.8 with the protein database from Uniprot (*Homo sapiens*, 16 July 2013, 88 354 entries). Maximum mass tolerance was set at 7 and 20 ppm for precursor and fragment ions, respectively. The threshold for the false discovery rate was 5% and protein quantification was set at minimum of two peptides identified for each protein.

Protein purification

The CSB-wt, CSB-PARr, and CSB fragments 230–1493, 360–1493, and 447–1493 aa were tagged at the N-terminal domain with GST and at the C-terminal domain with HIS10, expressed in Sf9 insect cells, and purified as described [61]. Proteins were eluted with Talon buffer containing 500 mM imidazole and dialyzed in storage buffer (20 mM Tris–acetate, pH 8.0, 200 mM NaCl, 10% glycerol, 1 mM Dithiothreitol (DTT).

Interaction assays

In cells: The GFP-tagged PARP1 or its fragments were transiently transfected in HEK PARP1-ko cells, and 72 h later harvested in ice-cold 1× PBS (500 × *g*, 10 min, 4°C). Where indicated, DNA damage was induced by UVC irradiation 30 min prior to harvesting cells. The cell pellet was suspended in buffer A [50 mM Tris, pH 7.5, 300 mM NaCl, 5 mM EDTA, 0.5 mM phenylmethyl sulfonyl fluoride (PMSF), 0.2% NP-40, 1× complete EDTA-free protease inhibitor (Roche)] and incubated for 20 min on ice. Cell debris was pelleted at 16 000 × *g*, 15 min, at 4°C and the lysate was diluted with buffer A without salt to a final 150 mM NaCl concentration. An equal protein content was incubated with the appropriate antibody overnight at 4°C under constant rotation. The protein complexes were pulled down with Dynabeads protein G magnetic beads (Invitrogen) for 1 h at 4°C under constant rotation. The beads were washed with TBS-T buffer (5 min, 4°C) and eluted with 2× Laemmeli (LB) sample buffer. The same protocol was followed for performing immunoprecipitation of endogenous PARP1 in HEK expressing GFP-CSB or its fragments. ***In vitro*:** We used recombinant human CSB (Origene, TP319020) and its fragments [61], recombinant automodified human PARP1 (Tulip, BioLabs, 2095), human PARP1 (Enzo Life Sciences, ALX-201-063 and [62] and its fragments: 1–327 (Creative Biomart, #PARP1-530H), 215–1014 (Antibodies-online, #2854042), 622–1014 (Antibodies-online, #666940), and GST tagged 379–494 aa to study the direct interaction of CSB–PARP1 [62]. The CSB or PARP1 was reacted with an equimolar amount of PARP1 or CSB protein or fragments at 25°C for 30 min. CSB antirabbit antibody H-300 (Santa Cruz) or PARP1 antimouse (F1-23) antibody was bound to Dynabeads Protein G magnetic beads (Invitrogen) in TBS-T with constant rotation for 1 h at ambient temperature. The beads were washed with TBS-T three times and added to protein reaction for 1 h on ice, mixing intermittently. The beads were washed three times with TBS-T, eluted with Laemmli buffer, the proteins separated on sodium dodecyl sulphate–polyacrylamide gel electrophoresis (SDS–PAGE), transferred on nitrocellulose, and probed with their antibodies. To study RNAPII–PARP1 interaction, the immunopurified RNAPIIS2 from HEK PARP1-ko cells was reacted with PARP1 and its fragments 1–327 (Creative Biomart, #PARP1-530H), 215–1014 (Antibodies-online, #2854042), 622–1014 (Antibodies-online, #666940), and GST 379–494 aa [62], as described above.

PAR assays

In vivo: The PARylated proteins in cells were detected as previously described [63] The cells were globally irradiated (30 J/m^2 UVC) or treated with Illudin S (30 ng/ml) and the whole cells extracts were prepared at specified time points by lysing the cells in sample buffer. Proteins were separated by SDS–PAGE, transferred on nitrocellulose membrane and probed with the indicated primary antibodies. ***In vitro*:** The ability of CSB to stimulate PARP activity was done by performing PARP1 activation assay in absence and presence of various equimolar ratio of full-length CSB or its fragments. A master mix with NAD^+ (Roche), PARP1, and Tris buffer (100 mM Tris, pH 8.0, 10 mM $MgCl_2$, 10% glycerol, 1.5 mM DTT) was distributed equally in tubes containing either CSB or its fragments. UVC-DNA that was prepared by irradiating 3.2 kb PBS-U6 plasmid with 5000 J/m2 UVC was added to each tube and incubated at 25°C for 30 min. The reaction was stopped by addition of 2× Laemmli buffer, the proteins separated on SDS–PAGE, transferred on nitrocellulose and probed with their antibodies.

The ability of CSB to bind free PAR was studied by dot-blot (nondenaturing condition) and South-Western assay (separation under denaturing conditions followed by renaturation before transfer) as described previously [41]. For the immune-dot-blot, PARP1, CSB-wt, CSB PARr, GST and BSA were spotted on a nitrocellulose membrane pre-wetted with TBS-T (10 mM Tris, 150 mM NaCl, 0.05% Tween 20). For South-Western blots, PARP1, BSA, CSB or its fragments were resolved on a 8% SDS–PAGE gel. The PAR resistant GFP-CSB and its wild-type form were immunopurified from U2OS CSB-ko cells stably expressing these constructs and the GFP-CSB fragments from HEK293 cells 48 h after transfection. The cells were lysed for 20 min on a rotating wheel at 4°C in 1 ml of Triton lysis buffer [25 mM Tris (pH 7.5), 500 mM NaCl, 0.5% triton, 5 mM EDTA, 0.5 mM PMSF, 10% glycerol and protease inhibitor cocktail (Roche)], followed by centrifugation for 15 min at 13 000 rpm at 4°C. The supernatants were trans-

ferred into fresh tubes and the cell extracts diluted 1:2 with triton lysis buffer without NaCl. The GFP proteins were immunoprecipitated by incubation with 25 µl prewashed GFP-trap beads (Bulldog bio) for 3 h at 4°C. After incubation, the beads were washed with 1.5 M NaCl Triton lysis buffer to disturb protein complexes and eluted proteins were resolved on a 6% SDS–PAGE. The proteins were renatured by soaking the gel in 20–30 ml of running buffer containing 5% β-mercaptoethanol for 1 h on a rocking platform, at ambient temperature, before transferring them on nitrocellulose. The nitrocellulose membranes were washed three times with TBS-T and incubated for 1 h at room temperature with 10–15 ml of TBS-T containing 250 nM purified PAR as described. The membranes were washed three times 10 min with TBS-T, followed by three washes with TBS-T containing 500 mM NaCl to remove the unbound and loosely bound PAR. The membranes were blocked with TBS-T containing 5% (wt/vol) non-fat milk powder and probed with anti-PAR (10H) antibody. The membranes were stripped at low pH (25 mM glycine, pH 2.0 with 1% SDS, 15 min at ambient temperature) and probed for PARP1, GFP, CSB, and GST using antirabbit antibodies.

Binding of proteins to DNA

The binding of PARP1 or CSB to UV-oligos immobilized on the magnetic streptavidin beads was studied as described previously [39]. The bead-bound oligos were reacted with PARP1 or CSB at 1:1 molar ratio in Tris buffer (100 mM Tris buffer, pH 8.0, 10 mM $MgCl_2$, 10% glycerol, 150 mM NaCl, 1.5 mM DTT, and protease inhibitor) at 25°C for 15 min. To study the effect of CSB PARylation on its DNA binding capacity, PAR was added to the DNA-CSB mix at 1:1:1 molar ratio and the reactions were carried out with or without 2 mM ATP at 30°C for 30 min. The unbound proteins were removed and the bound proteins were crosslinked to oligo with 1% formalin in Na-PO_4 reaction mixture for 10 min at ambient temperature. After quenching formalin with 250 mM Tris–HCl, pH 8.0, the beads were washed twice with Tris-reaction mixture and eluted with LB.

ATP Hydrolysis assay

The CSB-wt and PARr-CSB (50 nM) were mixed with 150 ng DNA and/or different amounts of PAR in MOPS Buffer (25 mM MOPS, pH 7.0, 100 mM KCl, 0.2% Tween 20, 1 mM DTT, 5 mM MgCl2, 0.1 µCi γ-^{32} P -ATP) and incubated at 37°C for 30 or 60 min. Where indicated, DNA or PAR were added 30 min after initiating the reaction. The aliquots of reaction mix removed at specified time points were quenched with an equal volume of 0.5 M EDTA. The ATP and inorganic phosphate (Pi) were separated by thin layer chromatography for 45 min in formic acid–LiCl buffer. The signals of ATP and Pi were quantified using phosphor-imager FLA-5100 (Fujifilm) and analysed using Image Reader FLA-5000 v1.0 software.

Statistics

For the RRS studies, three to five independent experiments were performed and the intensity of fluorescence from at least 200–1000 nuclei were analysed using Image J or with an in house written program which uses a modified version of IHC ToolBox plugin within Image J. The in-house program performs automatic detection of all the stained nuclei, automatic measurement of background stain intensity as well as automatic detection and intensity measurements of all the positive nuclei. To calculate the UDS-TCR, the fluorescence intensity at the damage site (at least 100 spots) was measured by Axiovert 200 (Zeiss) using the program AutoMeasure Plus of the software Axiovision version 4.7 and expressed as pixel per area followed by the subtraction of the background intensity detected outside of the spots from an identic area in the nucleus. For clonogenic survival, the colonies from a six-well cluster by treatment group of two independent experiments were counted with GeneTools (Syngene). For each cell line, a pixel cut-off defined as the aria occupied by a colony formed by at least 35–50 cells in untreated condition was applied to the treated groups. Results are expressed as mean ± SEM. The statistical significance of difference was determined by unpaired two-tailed *t*-tests and ∗ refers to significant *P*-values <.05.

Results

Increased susceptibility to Illudin S and inefficient TCR in PARP1-impaired cells

TCR-deficient cells are sensitive to DNA damage by Illudin S, while GGR-deficient cells are not [64, 65]. Therefore, to assess the potential involvement of PARP1 in TCR while excluding its role in GGR, we compared Illudin sensitivity of GMU6 human skin fibroblasts after treatment with PARP-inhibitor or with its matched pair of PARP1-knockdown GMshPARP1 cells. To confirm that Illudin S preferentially activates the TCR pathway in our model, we compared the recruitment of GGR-specific DDB2 and TCR-specific CSB proteins to chromatin fraction of the GMU6 cells treated with Illudin S or UVC. These cells respond to UVC by recruiting DDB2 and CSB to the chromatin fraction but recruit only CSB after Illudin S treatment (Supplementary Fig. S1A). We also confirmed that DNA damage by Illudin S treatment resulted in PARylation of proteins which could be suppressed by PARPi (Supplementary Fig. S1B). In line with a role in TCR, we found that PARPi or PARP1-kd by shRNA (shPARP1) significantly reduced the clonogenic survival of GMU6 cells after Illudin S (Fig. 1A). The PARP1-ko also strongly sensitized the U2OS cells to Illudin S, albeit not to the same extent as TCR-deficient U2OS CSA-ko cells (Fig. 1B). The increased susceptibility of PARP1-ko cells to Illudin S has also been reported in previous genome-scale CRISPR-screens in RPE1 cells [52]. These results indicate a role for PARP1 and PARylation in facilitating TCR.

To further investigate this potential role of PARP1 in TCR, we employed an Recovery of RNA synthesis (RRS) assay that monitors transcription restart after the initial DNA damage-induced global transcription arrest [66, 67]. In GMU6 cells, a strong signal for RNA synthesis prior to Illudin S treatment was significantly suppressed at 3 h, followed by nearly full recovery of transcription by 24 h (Fig. 1C). In shPARP1 cells, the transcription was strongly reduced until 6 h and only partially recovered until 24 h, unlike CS-B deficient cells in which there was no recovery until 24 h. Treatment with PARPi also led to a significant reduction in transcription recovery, although milder than that observed after PARP1 knockdown at 24 h (Fig. 1C). The PARP1-ko in GM637 cells also decreased transcription recovery up to 24 h after Illudin S treatment (Supplementary Fig. S1C). Lastly, we used the RRS assay to monitor TCR after UVC treatment, because this assay re-

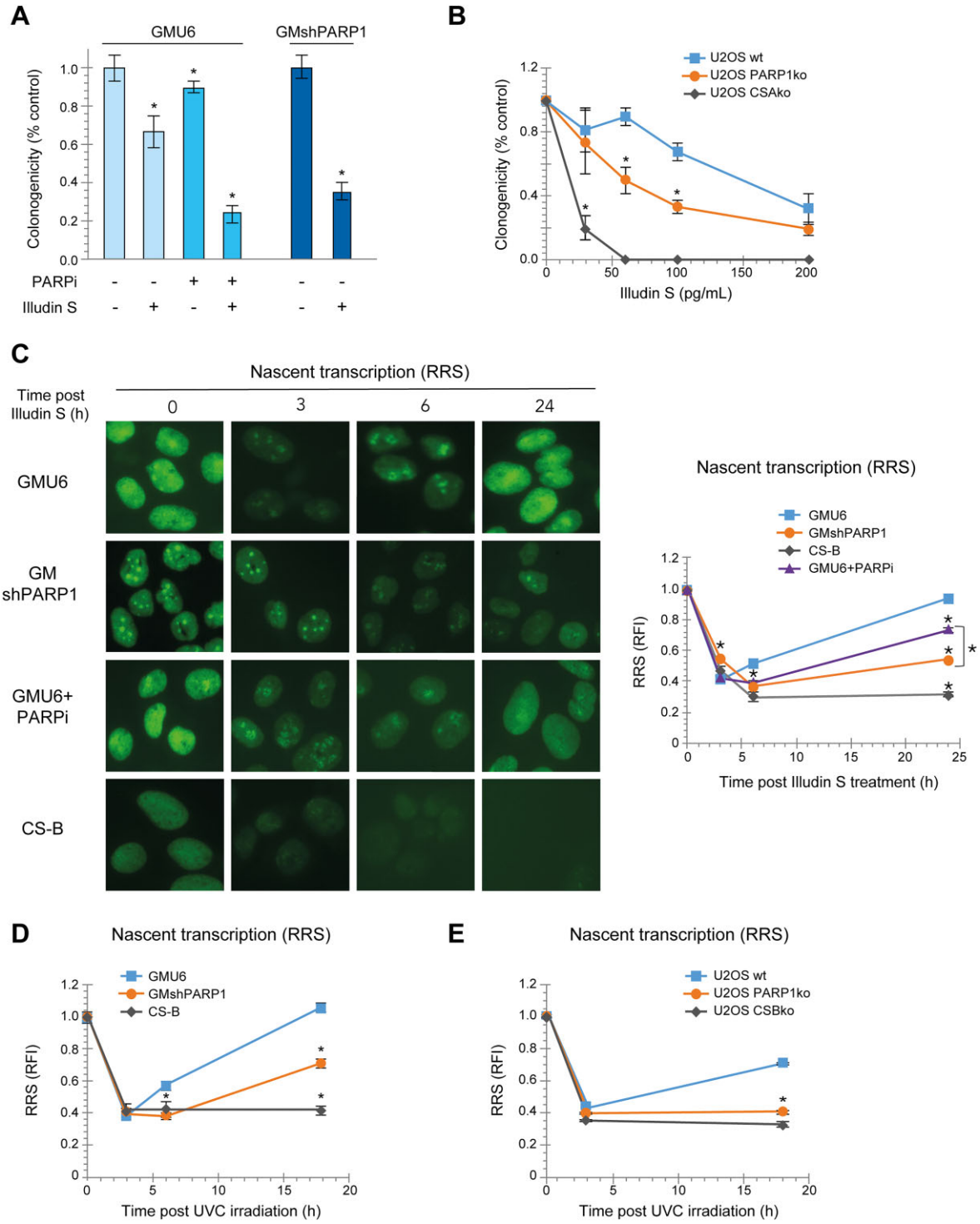

Figure 1. Increased susceptibility to Illudin S and inefficient RRS in PARP1-impaired cells. (**A, B**) PARP1 depletion or inhibition reduces the clonogenic survival of cells after Illudin S. (**A**) Clonogenic survival of GMU6 cells to Illudin S (1 ng/ml) for 24 h without or with 2 μM PARPi ABT-888 or PARP1-kd (GMshPARP1). Bars represent mean ± standard deviation (SD; $n = 3$). Note: In all panels of this and subsequent figures, ∗ denotes statistically significant difference with unpaired two-tails *t*-test (*P*-value <.05). (**B**) Clonogenicity of U2OS cells with indicated genotypes to dose-response of Illudin S ($n = 4$). (**C–E)** PARP1-impaired cells exhibit reduced RRS after DNA damage. (**C**) Images of GMU6 cells without or with PARPi, GMshPARP1, and CS-B cells 1 h after EU labelling at specified time of Illudin S treatment. The data of three biological replicates is expressed as mean ± standard error (SE) of relative fluorescence intensity (RFI, arbitrary units). Note that the error bars are smaller than the time point markers. (**D**, **E**) As in panel (C), but after UVC irradiation (10 J/m^2) in GMU6 (**D**) and U2OS (**E**) cells with indicated genotypes.

flects repair occurring only in the transcribed strand of the transcriptionally active gene. We noted that even after UVC treatment, transcription recovery was significantly suppressed up to 18 h in GMshPARP1 (Fig. 1D), PARP1-ko GM637 cells (Supplementary Fig. S1D), and in PARP1-ko U2OS cells (Fig. 1E). Thus, PARPi or PARP1-knockdown or knockout in two different cell lines significantly decreased transcription recovery after UV, which is a hallmark of defective TCR [68].

Interaction of PARP1 with RNAPII before and after UV or Illudin S-induced DNA damage

To understand the potential role of PARP1 in TCR, we used the proximity-dependent biotin identification (Bio-ID) technique with PARP1 fused to Bio-ID [43] to identify PARP1-interacting partners in TCR. The MS-MS analyses of streptavidin IP-eluates of chromatin fractions of these cells revealed that nine out of 12 members of the RNAPII complex were biotinylated before and after UVC irradiation (Fig. 2A), suggesting their close interaction during normal transcription and during TCR. In addition, some of the NER proteins and chromatin remodelling factors also displayed increased biotinylation following UVC irradiation. Thus, our Bio-ID approach revealed that PARP1 is in close contact with RNAPII in undamaged cells and is present when RNAPII stalls at DNA lesions.

We first examined the mode of interaction between PARP1 and RNAPII. There are two forms of RNAPII, the nonphosphorylated RNAPIIa initiates at the transcription start site, whereas the phosphorylated form of RNAPII (RNAPIIo) is the elongating form in gene bodies. Using antibody that detects both forms of RNAPII, we detected only the RNAPIIo before and after UV irradiation after pull-down of PARP1 from the chromatin fraction of GMU6 cells (Supplementary Fig. S2A). The RNAPIIo fraction consists of promoter-proximally paused RNAPII phosphorylated at Ser5 (RNAPIIS5) or elongating RNAPII carrying additional serine 2 phosphorylation (RNAPIIS2) [69]. In the BioID-PARP1 cells, the IP with RNAPIIS2-specific antibody pulled-down PARP1 both before and after irradiation, but CSB only after UV irradiation (Fig. 2B). Even in the GMU6 cells expressing endogenous PARP1, the reciprocal IP for PARP1 and RNAPIIS2 confirmed their interaction before and after UV irradiation (Fig. 2C and Supplementary Fig. S2B).

The recruitment of TCR protein complex at the stalled RNAPII is dependent on CSB, hence we examined whether CSB plays any role in the interaction between PARP1 and RNAPII specifically after DNA damage. We used CSB-ko GMU6 cells (Fig. 2D, top left panel) and confirmed that these cells were TCR deficient with a severely suppressed capacity for RRS up to 24 h after UV irradiation (Fig. 2D, bottom left panel). The absence of CSB in these cells did not decrease the interaction of PARP1 with RNAPIIS2 before or after UV irradiation, indicating that their interaction even after DNA damage is independent of CSB (Fig. 2D, right panel). We also confirmed in Illudin S-treated GMU6 cells that PARP1 interacts with RNAPIIo both before and after treatment (Fig. 2E, top panel) and more specifically with the RNAPIIS2 form (Fig. 2E, bottom panel).

To gain more insights into the physical interaction of PARP1 with RNAPIIo, we used PARP1-ko HEK cells (Supplementary Fig. S2C) to express GFP-tagged PARP1 or its fragments as well as the catalytically inactive PARP1 (PARP1-CI) (Fig. 2F, top panel). The RNAPIIS2-IP revealed a strong interaction with the full length PARP1 and its N-terminal fragment (1–232 aa), but a weak or no interaction with other fragments of PARP1 spanning 337–1014 aa or with the GFP-tag (Fig. 2F, bottom panel). Interestingly, the enzymatically inactive PARP1-CI also interacted robustly with RNAPIIS2 in the unirradiated cells. Moreover, even after UV irradiation, there was no change in the profile of interaction of RNAPIIo with the active and inactive PARP1 or PARP1 fragments (Supplementary Fig. S2D). Thus, neither DNA damage nor the catalytic activation of PARP1 to form PAR were required for the initial physical interaction between PARP1 and RNAPIIo in the cells. Finally, in an *in vitro* assay with purified PARP1 and its four overlapping fragments, we confirmed that the immunopurified RNAPIIS2 obtained from PARP1-ko HEK cells binds strongly with PARP1 and its N-terminal DBD fragment (1–327 aa), weakly with 215–1014 aa fragment but not with the with fragments after 379 aa (Fig. 2G). Thus, the interaction of PARP1 mainly via its N-terminal domain with RNAPIIo is independent of CSB or catalytic activation of PARP1.

PARP1 and PARylation promote the interaction of CSB with RNAPII to initiate TCR

The stabilization of CSB with the lesion-stalled RNAPII is essential for the initiation of TCR. Since PARP1 is also present with RNAPII at the DNA lesion site, we examined by co-IP studies if CSB recruited to DNA lesion-stalled RNAPII also interacts with PARP1. The pull-down of PARP1 from the chromatin fraction of GMU6 cells revealed its interaction with CSB only after UV irradiation, unlike its damage-independent interaction with RNAPIIo (Fig. 3A). The identification of a DNA damage-induced interaction of CSB with PARP1 by co-IP but not by Bio-ID-PARP1 approach is due to the limitation of the Bio-ID method that requires long biotin labelling time which often excludes proteins that react briefly with PARP1 after DNA damage, as we noted earlier for the DDB2–PARP1 interaction during GGR [43]. The pull-down of GFP-tagged CSB from U2OS cells confirmed its interaction with RNAPIIS2 as well as with PARP1 only after UV irradiation (Fig. 3B).

We next used purified proteins to explore a direct interaction of CSB *in vitro* with PARP1 and PARylated PARP1, and observed that CSB-IP pulls down both native and PARylated PARP1 (Fig. 3C), indicating that auto-PARylation of PARP1 would not disrupt its interaction with CSB. To identify the domains of PARP1 involved in this interaction, we reacted PARP1 or its four overlapping fragments with full length CSB (Fig. 3D). The IP of CSB showed its interaction with full-length PARP1 as well as a fragment spanning aa 215–1014. In contrast, fragments spanning 1–327 aa (DBD), 379–494 aa (BRCT domain), or 622–1014 aa (catalytic domain) did not interact with CSB. Thus, PARP1 interacts with CSB via its central region of 495–621 aa containing the WGR domain. These results suggest that PARP1 can simultaneously interact with RNAPII via its N-terminal DBD and with CSB via its WGR domain.

Next, we examined whether the interaction of CSB with lesion-stalled RNAPII is influenced by PARP1 and PAR formation (Fig. 3E). The pull-down of RNAPIIS2 revealed that both PARPi and shPARP1 decreased the UV-induced interaction be-

A

Gene	Signal Intensity		Ratio UV/C
	Chr-C	Chr-UV	
PARP1	9.80E+09	1.70E+10	1.7
RNA polymerase II complex			
POLR2A	1.10E+09	9.06E+08	0.8
POLR2B	5.99E+08	6.27E+08	1.0
POLR2C	3.64E+08	1.01E+08	0.3
POLR2E	5.07E+07	6.10E+07	1.2
POLR2H	5.60E+07	7.10E+07	1.3
POLR2I	4.98E+07	2.88E+07	0.6
POLR2L	2.24E+08	1.92E+08	0.9
POLR2J POLR2J3; POLR2J2	1.99E+07	1.08E+07	0.5
POLR2K	1.07E+07	1.49E+07	1.4
NER related proteins			
ERCC3	0.00E+00	2.90E+07	∞
DDB1	1.78E+07	1.49E+08	8.4
USP7	1.97E+07	4.17E+07	2.1
Chromatin remodeling factors			
SUPT16H	1.97E+07	2.85E+08	14.5
SSRP1	1.29E+07	3.01E+08	23.3
HIRA	3.49E+08	2.81E+08	0.8
SMARCA5	1.65E+09	2.47E+09	1.5
SMARCA4	1.33E+09	8.25E+08	0.6
NAP1L1	2.97E+07	2.36E+08	7.9

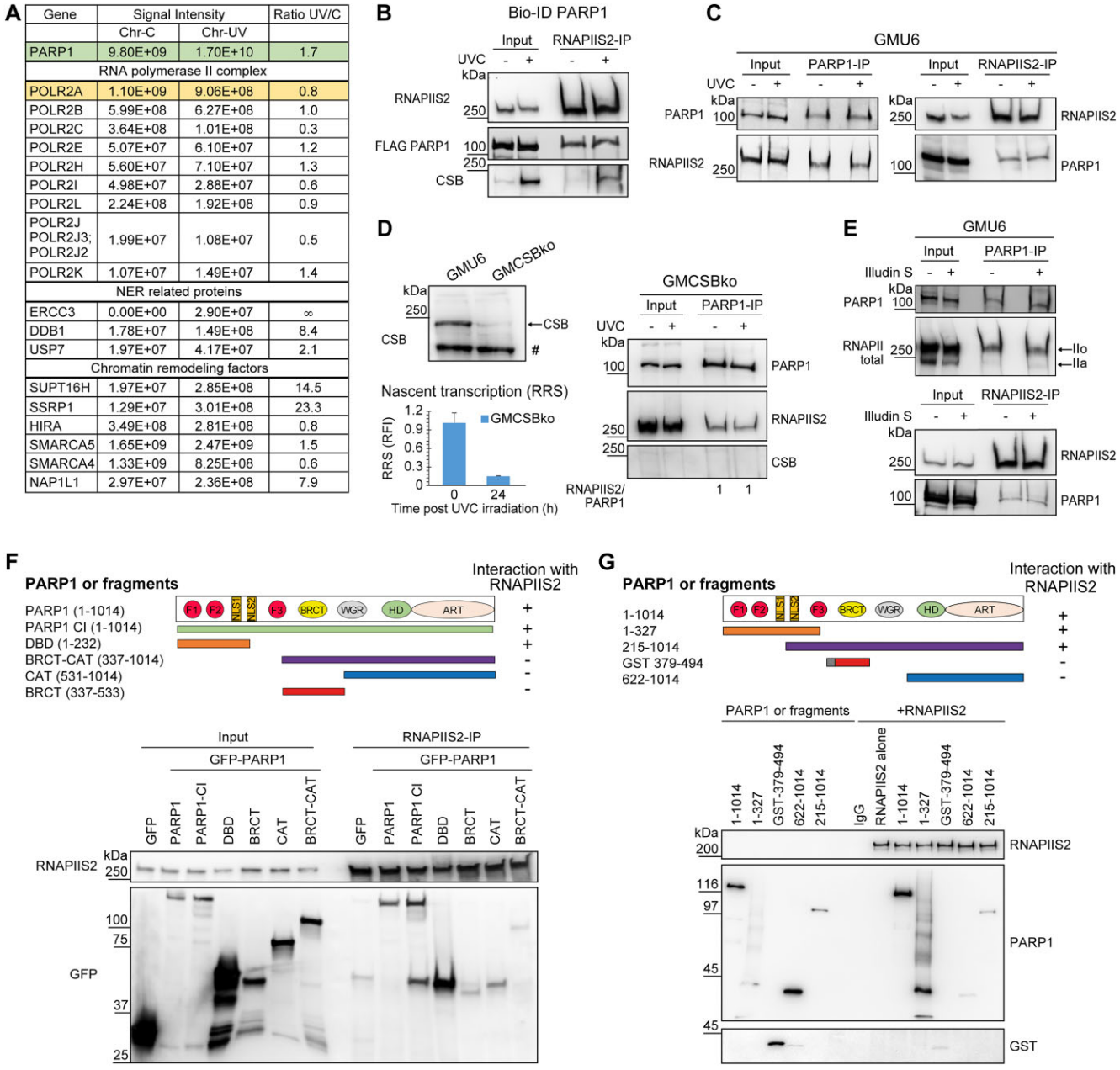

Figure 2. PARP1 interacts with RNAPIIo before and after DNA damage. (**A**) Bio-ID-PARP1 screen identifies the interaction of PARP1 with multiple subunits of RNAPII, NER, and chromatin remodeling factors. The chromatin fraction of mock and UVC (30 J/m^2) irradiated Bio-ID-PARP1 cells were subjected to streptavidin-IP followed by MS-MS analyses for detection of biotinylated partner proteins ($n = 2$). (**B, C**) DNA-damage independent interaction of PARP1 with RNAPIIo. (**B**) IP for RNAPIIS2 in control and UVC-treated Bio-ID-FLAG-PARP1 chromatin fractions before or 30 min recovery after UVC (30 J/m2). (**C**) Reciprocal IP for PARP1 and RNAPIIS2 in the chromatin fractions of GMU6 cells before and 30 min after UVC (30 J/m^2). (**D**) Interaction of PARP1 with RNAPIIS2 in the absence of CSB. The GMU6 CSB-ko cells (left panel) were irradiated with UVC (30 J/m^2) and PARP1-IP was carried out before and 30 min after irradiation (right panel). The ratio of RNAPIIS2/PARP1 was calculated from immunoblots of four independent experiments. (**E**) PARP1 interacts with RNAPIIo form: The chromatin fractions of GMU6 cells treated with Illudin S (30 ng/ml, 30 min) were subjected to reciprocal IP for PARP1, and RNAPIIS2 followed by detection of specified target proteins. (**F, G**) RNAPIIo interacts with the N-terminal DBD of PARP1. (**F**) The whole cell extracts of HEK293 PARP1-ko cells transiently transfected with GFP-tagged PARP1 or its fragments (pictogram) were subjected to RNAPIIS2-IP and probed for GFP and RNAPIIo. (**G**) The bead-bound RNAPIIS2 obtained by IP-purification from HEK293 PARP1-ko cells was reacted for 20 min with purified full-length PARP1 and its fragments (pictogram) followed by immunoblotting with indicated antibodies.

tween RNAPII and CSB. Interestingly, CSB was present in the chromatin fraction in both PARPi or shPARP1 cells, as seen in the input lanes of these samples (Fig. 3E) and in a 24 h time-course following CSB movement to the chromatin fraction of UV-irradiated GM cells (Supplementary Fig. S3A and B). Furthermore, PARP1-ko in GM cells also reduced the UV-induced interaction of RNAPIIo with CSB (Supplementary Fig. S3C). Thus, despite the presence of CSB in the chromatin fraction, its UV-induced interaction with RNAPIIS2 was reduced in the PARP1-knockout or knockdown cells or in cells treated with PARPi. To support this observation made with UV-irradiated cells, we treated GMU6 cells with Illudin S, and the reciprocal IP for RNAPIIS2 and CSB confirmed that PARPi treatment significantly suppressed the interaction of CSB with RNAPII

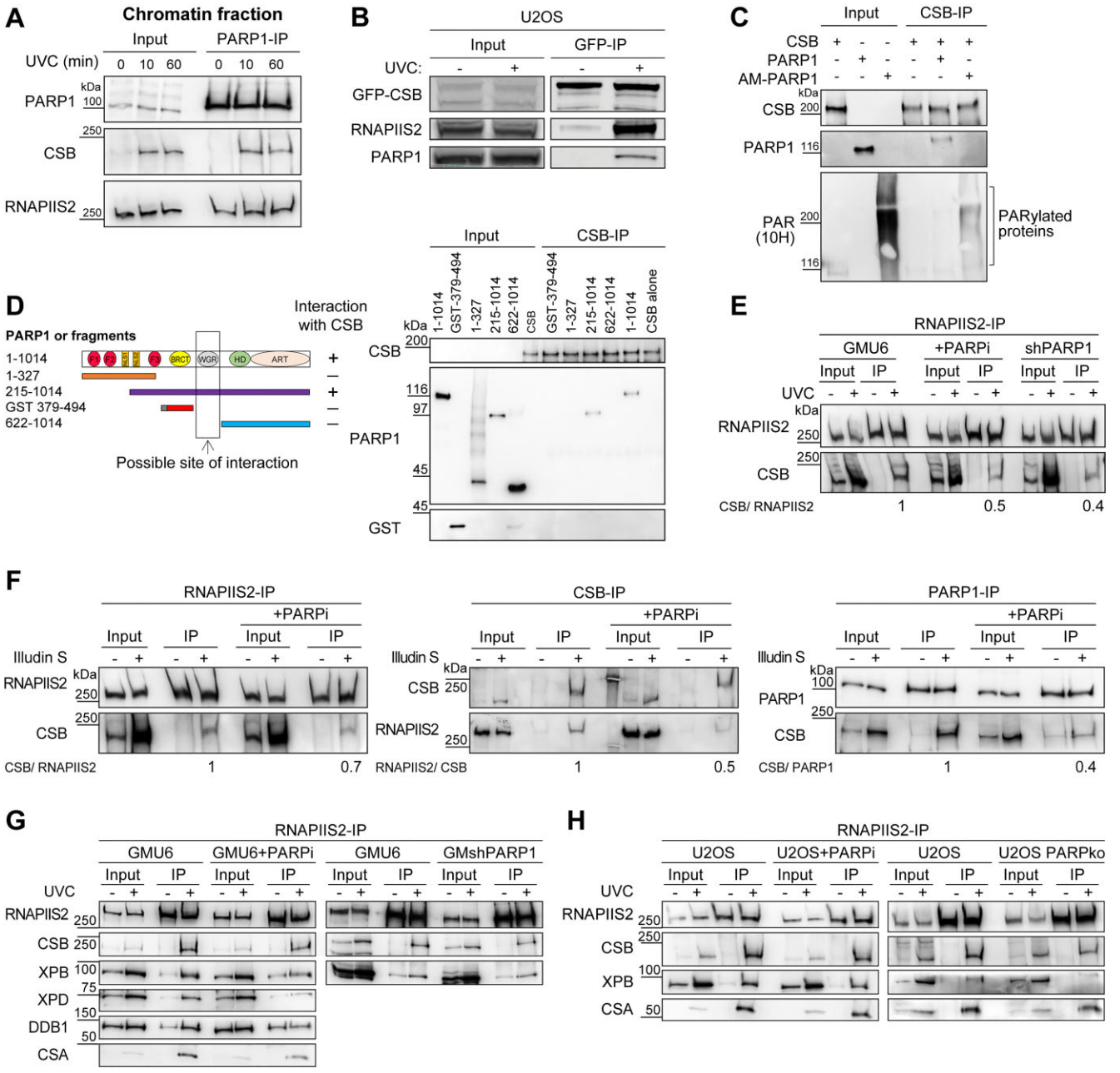

Figure 3. PARP1 and PARylation mediate CSB interaction with RNAPIIo after DNA damage. (**A, B**) PARP1 interaction with CSB only after DNA damage. (**A**) IP of PARP1 in the chromatin fractions of GMU6 cells prepared before or after UVC (30 J/m^2). (**B**) U2OS CSB-ko cells rescued with GFP-CSB-wt were irradiated with UVC (20 J/m^2) and the chromatin fractions subjected to GFP-IP. (**C, D**) Direct interaction of CSB with WGR domain of PARP1. (**C**) CSB interacts with both PARylated and unmodified PARP1 *in vitro*. Purified CSB was reacted with unmodified or PARylated PARP1 and subjected to CSB-IP. (**D**) The PARP1 and its four partially overlapping fragments (pictogram) were reacted *in vitro* with purified CSB followed by CSB-IP. (**E–H**) PARP1 depletion or inhibition reduces the interaction of CSB with RNAPIIo resulting in an inefficient recruitment of downstream TCR proteins. (**E**) IP of chromatin-bound RNAPIIS2 following treatment with UVC (30 J/m2) of GMU6 cells with or with 2 μM PARPi (olaparib) treatment and PARP1-depleted GMshPARP1. (**F**) GMU6 cells with or without PARPi (olaparib 2 μM) were treated with 30 ng/ml Illudin S, and the chromatin fractions were subjected to IP for RNAPIIS2, CSB, and PARP1. (**G, H**) PARP1-ko or PARP1-kd or treatment with 100 nM PARPi BMN637 decreases recruitment of downstream TCR proteins in GMU6 (**G**) or U2OS cells (**H**). The chromatin fractions from these cells 1 h after exposure to UVC (30 J/m2) were subjected to RNAPIIS2-IP. The ratios in panels (E) and (F) were calculated from the given experiment, and is representative of three independent experiments with similar result.

(Fig. 3F, left and middle panel). Moreover, PARP1-IP revealed that PARPi also suppressed the interaction of CSB with PARP1 (Fig. 3F, right panel). To ascertain that PARylation formed by PARP1 plays a key role in the CSB–RNAPII interaction, we rescued HEK PARP1-ko cells with wild type or catalytically inactive (CI) PARP1 (Supplementary Fig. S3D). After exposure to UVC, the RNAPII-IP revealed a reduced interaction of CSB with RNAPII in CI-PARP1 expressing cells (Supplementary Fig. S3E). Thus, PARP1 and its catalytic activity play a key role in stabilizing the interaction of CSB with lesion-stalled RNAPII. A consequence of the reduced interaction between RNAPII and CSB in PARP1-impaired cells would be an inefficient recruitment of downstream TCR proteins. The pull-down of RNAPIIS2 in GMU6 (Fig. 3G) and

U2OS (Fig. 3H and Supplementary Fig. S3F) revealed that PARPi and knockdown or knockout of PARP1 reduced the UV-dependent interaction of RNAPIIo with key TCR downstream proteins, such as DDB1, CSA, XPB, and XPD. Thus, PAR formed by PARP1 plays a key role in promoting the interaction between RNAPII and CSB, which is essential for recruitment of downstream TCR proteins.

CSB stimulates PARP1 activity and PARylation of CSB leads to efficient TCR

Having found that PARP1 and PARylation regulate the interactions of CSB with RNAPIIo, we next explored the underlying mechanism. The WGR domain of PARP1 is implicated in stimulating PAR synthesis by PARP1 following DNA damage [70]; hence, we examined whether the interaction of CSB with this domain regulates the catalytic activity of PARP1. Knockout of CSB in GMU6 cells significantly reduced the signal for PAR-modified proteins after Illudin S or UVC treatment, suggesting that the CSB–PARP1 interaction stimulates PARylation (Fig. 4A). To understand how CSB stimulates the catalytic activity of PARP1, we examined whether PARP1 or CSB could alter each other's capacity to bind to UV-damaged DNA such as a biotinylated 60-mer oligonucleotide with a defined CPD lesion [39]. Interestingly, the inherent capacity of PARP1 to bind to the CPD oligo was increased in the presence of CSB (Fig. 4B), which coincided with a stimulation of PARP1's catalytic activity with increasing dose of CSB to form more PAR in the presence of UV-damaged circular plasmid DNA at molar ratio from 0.5:1 to 2:1 (Fig. 4C). In contrast, an earlier study showed that CSB suppresses PARP1 activation by UV-irradiated double-stranded DNA *in vitro*; and that CS-B cells have very high levels of PAR even without any DNA damage [58]. Therefore, differences in our results could be due to use of cellular models with different levels of endogenous PAR formation and different type of DNA used for activation of PARP1 *in vitro*.

To pinpoint the domain of CSB that is required for binding to PARP1 under cellular conditions, we expressed GFP tagged full-length CSB and three nonoverlapping fragments representing the N-terminal domain (1–455 aa), the middle region (455–1221 aa) and the C-terminal domain (1221–1493 aa) in HEK293 cells. The PARP1-IP of total cell extracts revealed that all proteins associated with PARP1 except the N-terminal fragment of CSB (Fig. 4D). However, Thorsland *et al*. [71] had earlier shown that N-terminal domain of CSB interacts with PARP1. This led us to examine the interaction of CSB with PARP1 using an alternative approach. We reacted *in vitro* purified PARP1 with purified CSB or its three N-terminal deletion fragments starting at 230, 360, and 447 aa. The PARP1-IP revealed that all three CSB fragments bind to PARP1, indicating that the ability of CSB to bind to PARP1 is not dependent on its N-terminal domain from 1–447 aa (Fig. 4E, left panel). Moreover, all three N-terminal deletion fragments could not only bind to but also increased PARylation activity of PARP1, with the strongest activation seen with fragment 447–1493 (Fig. 4E, right panel). Thus, using two different series of fragments of CSB and their reaction with PARP1 *in vitro* and in cells, we show that CSB does not bind to PARP1 via its N-terminal domain, but through its regions in 455–1493 aa, which also results in stimulation of catalytic activity of PARP1 to form more PAR.

The CSB was earlier shown to be PARylated *in vitro*, and this was shown to play a role in oxidative damage responses [71]. This led us to examine whether the interaction of CSB with PARP1 leads to its PARylation during TCR. In Illudin S-treated GM cells, the PAR-IP of chromatin extract pulled-down both PARP1 and CSB among the PARylated proteins (Fig. 4F, top panel). To confirm direct PARylation of CSB, we reacted purified CSB, PARP1, BSA, and GST spotted on a nitrocellulose membrane with purified PAR and noted that free PAR strongly binds to PARP1 and CSB but not to control BSA and GST tag (Fig. 4F, bottom panels), confirming that CSB can noncovalently bind to PAR. Moreover, we also noted that the full-length CSB and its fragment from 230–1493 strongly bind to PAR, whereas the fragment 360–1493 was a weak acceptor of PAR (Fig. 4G, left panel). Finally, we reacted immunopurified GFP-CSB and three nonoverlapping fragments (1–455, 456–1221, and 1221–1493 aa) with free PAR in a SouthWestern assay and observed that PAR-binding affinity was strongest for the N-terminal 1–455 aa fragment followed by weaker binding by the C-terminal 1221–1493 aa fragment (Fig. 4G, right panel). Our results show that CSB associates noncovalently with PAR mainly through the N-terminal domain from 230–360 aa, with minor PARylation occurring in the C-terminal domain from 1221–1493 aa.

Two PBM have been identified in the N-terminal domain of CSB [30, 58]. We mutated two key Lys residues to Ala in each of the two PBMs of CSB from 292–299 and 333–340 aa (Fig. 4H, top panel); and created stable clones expressing this mutant CSB in U2OS CSB-ko cells. The PAR-acceptance capacity of the mutant and wild type CSB immunopurified under stringent conditions from their respective U2OS cells using a SouthWestern assay confirmed that mutant CSB was resistant to accept free PAR (Supplementary Fig. S4A, left panel). Furthermore, using insect cells, we expressed and purified the mutant and wild type CSB proteins and confirmed using a dot-blot assay that the mutant CSB was a weak acceptor of PAR, confirming the N-terminal domain of CSB as a major PAR-acceptor site (Supplementary Fig. S4A, right panel).

Next, we examined whether the TCR events would unfold differently in response to UV in the cells expressing N-terminal PAR-resistant-CSB (PARr-CSB). The RNAPIIS2-IP from chromatin revealed decreased association of PARr-CSB with RNAPII as compared to CSB-wt, which culminated in a reduced recruitment of downstream TCR proteins (Fig. 4H, bottom panel). Interestingly, PARP1-IP in these cells showed that the wt-CSB and the PARr-CSB were equally proficient in interacting with PARP1 (Supplementary Fig. S4B). Thus, the inefficient interaction of the N-terminal PARr-CSB with RNAPII was not due to its inability to associate with PARP1 but due to its resistance to accept PAR in its N-terminal domain.

Finally, we measured TCR efficiency through RRS assays in U2OS CSB-ko cells rescued with either CSB-wt or PARr-CSB (Fig. 4I). At 18 h, both PARr-CSB clones had significantly suppressed recovery of RRS compared with CSB-wt cells, albeit slightly less severely than CSB-ko cells. Lastly, we examined whether the reduced TCR capacity of PARr-CSB cells would render them sensitive to Illudin S. Indeed, expression of PARr-CSB caused strong sensitivity to Illudin S, although not to the same extent as CSB-ko cells (Fig. 4J). Thus, after DNA damage, CSB associates with and stimulates the catalytic activity of PARP1, leading to PARylation of CSB at the

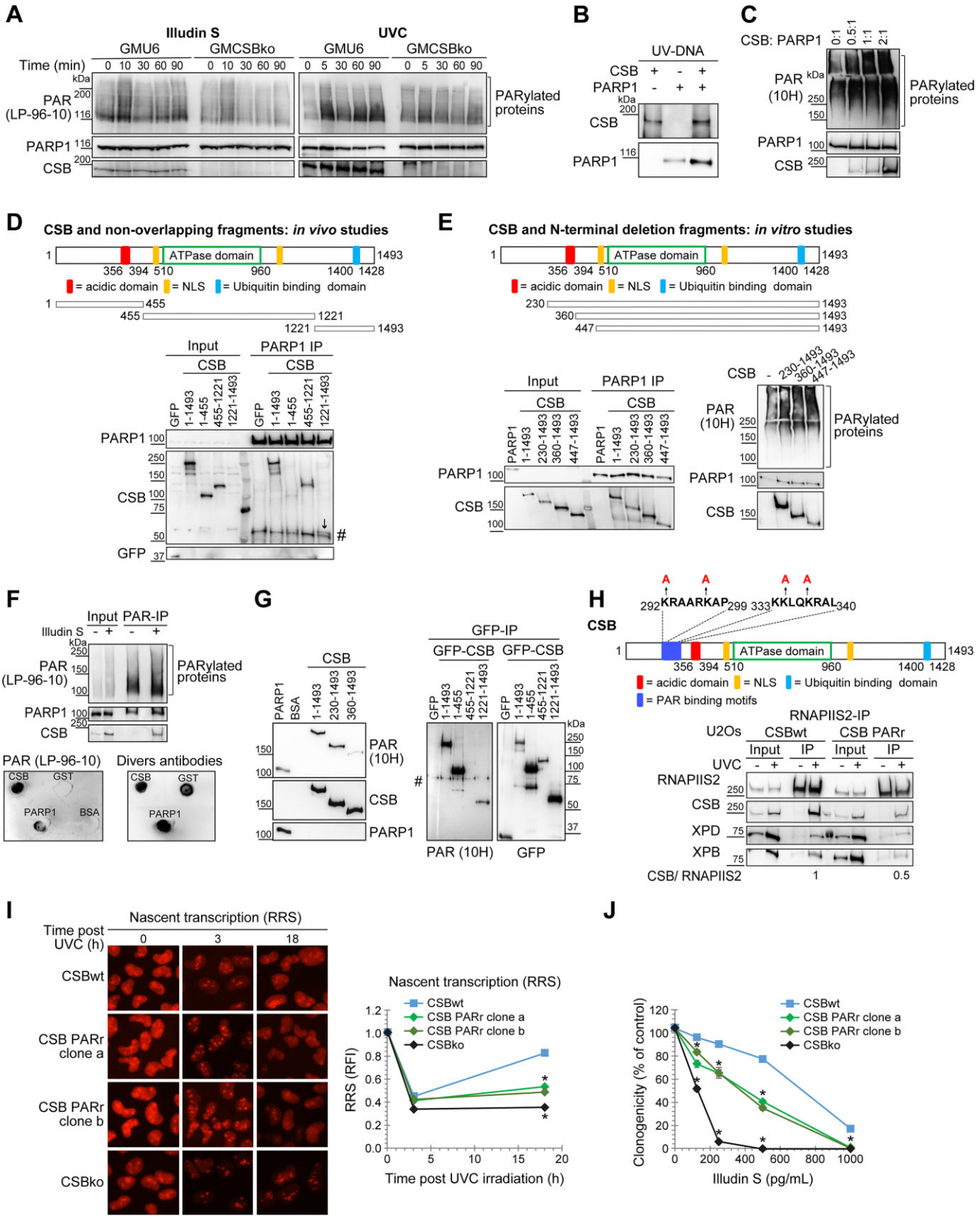

Figure 4. CSB stimulates PARP1 and PARylation of CSB improves TCR-efficiency. (**A-C**) Binding of PARP1 to damaged DNA and its catalytic activation is improved by CSB. (**A**) GMU6 and CSB-ko GMU6 cells were mock or treated with 30 ng/ml Illudin S (left panel) or 30 J/m^2 UVC (right panel), and whole cell extracts at specified time points were immunoblotted for PAR, CSB, and PARP1. (**B**) Purified PARP1 and CSB were reacted individually or together with biotin-tagged 60-mer UV-oligonucleotide bound to streptavidin-beads. (**C**) Purified PARP1 was reacted with CSB in specified ratios and subjected to *in vitro* PARylation assay. (**D, E**) CSB domains that interact with PARP1 in cells and *in vitro*. (**D**) HEK293 cells were transiently transfected with GFP-CSB and its nonoverlapping fragments for 48 h and whole cell extracts were subjected to PARP1-IP. # refers to nonspecific binding. (**E**) The purified CSB and

N-terminal domain, which facilitates the stable interaction of CSB with RNAPII, resulting in efficient TCR and survival of cells.

PAR suppresses ongoing DNA-dependent ATPase activity of CSB but not its binding to DNA

For lesion recognition, CSB binds to DNA behind RNAPII, and pulls the template strand in an ATPase-dependent manner, pushing RNAPII forward. When CSB fails to push RNAPII beyond the lesion site, it initiates TCR [10]. Considering the important role of PARylation of CSB in stabilizing the CSB–RNAPII interaction in cells, we examined the impact of PAR on the ATPase activity of CSB in an *in vitro* assay. The addition of DNA strongly stimulated the ATPase activity of CSB, which was significantly suppressed by addition of free PAR (Fig. 5A and Supplementary Fig. S5A). Moreover, we noted that CSB that was reacted with free PAR at the beginning of the ATPase assay was unable to hydrolyse ATP when DNA was added after 30 min, whereas PAR addition at 30 min in the reaction of CSB with DNA suppressed further ATPase activity of CSB (Fig. 5A). We confirmed using a streptavidin bead-bound 60-mer DNA with a defined CPD lesion that the reduction in ATPase function of CSB was not due to the interference in binding of CSB to DNA by PAR and/or ATP (Supplementary Fig. S5B). Interestingly, the addition of PARP1 or PARP1 + NAD that would result in catalytic activation of PARP1 and formation of autoPARylated PARP1 did not inhibit the DNA-stimulated ATPase function of CSB (Supplementary Fig. S5C). Together these results indicate that the cellular conditions that favour the availability of free PAR in the vicinity of DNA damage would suppress the ATPase activity of CSB.

Since PAR binds to CSB mainly in its N-terminal domain and to a lesser extent in the C-terminal domain, we used purified wild type CSB and N-terminal PARr-CSB to examine which of the two PARylation sites play a role in suppressing ATPase function of CSB. In an vitro assay we observed that ATPase function of both wt and PARr-CSB were equally suppressed by addition of free PAR in a dose-dependent manner (Fig. 5B), indicating that the inhibition of CSB's ATPase activity was not induced via predominant PARylation of N-terminal domain but via minor PARylation at C-terminal domain of CSB. Moreover, the PAR-dose dependent increase in inhibition of ATPase activity of CSB, indicates that a significant accumulation of free PAR is required to fully suppress ATPase function of CSB. Collectively, these results indicate that the major PARylation of CSB at its N-terminal domain is important for stabilization of CSB with RNAPII and for downstream events of TCR and cell survival (Fig. 4), whereas the minor PARylation of CSB in the C-terminal domain suppresses the ATPase activity of CSB (Fig. 5A and B, and Supplementary Fig. S5A), which is necessary to launch TCR after ATP-dependent lesion recognition step is completed by CSB.

PAR catabolism by PARG is required for the CSB–RNAPII interaction and efficient TCR

The influence of PAR binding to CSB in promoting its interaction with RNAPII and in inhibiting its ATPase function led us to examine whether PARG, the major PAR-catabolizing enzyme that releases free PAR from initially PARylated substrates influences TCR. We first confirmed that PARGi significantly enhanced the signal for PARylated proteins after UV irradiation, which was absent in shPARP1 cells (Supplementary Fig. S5D), indicating the major role of PARP1 and PARG in synthesis and catabolism of PAR, respectively, in these cells. More importantly, PARGi treatment suppressed the UV-induced interaction of CSB with RNAPIIS2 (Fig. 5C), similar to that seen when PAR formation was blocked by PARPi. The reduced interaction between RNAPII and CSB by PARGi has functional consequence for TCR, since we noted a similar defect in transcription recovery in both PARPi and PARGi-treated cell at 18 h after UVC irradiation (Fig. 5D).

PARP1, PAR and PARylation of CSB are required for efficient UDS-TCR in human cells

Finally, we examined the influence of PARP1 and PAR metabolism on TCR-dependent DNA repair. To this end, we measured TCR-related unscheduled DNA synthesis (UDS-TCR) that replaces the excised damaged single-strand containing the DNA lesion [66, 72]. To measure DNA synthesis only after TCR, we locally UV-irradiated [37, 73] XP-C cells followed by incubation with Click-iT EdU [74]. The specificity of the method was validated with GGR- and TCR-deficient cell lines and with transcription inhibitors (Supplementary Fig. 5E–H). To study the influence of PARP1 in this process, we generated shPARP1 XP-C cells. We observed an inefficient RRS (Supplementary Fig. S5I) and a significantly decreased UDS-TCR in these cells as compared to wild-type XPCU6 clones (Fig. 5E). Furthermore, the UDS-TCR from 3 to 6 h in XP-C cells depleted for PARP1 or in the presence of PARPi or PARGi also exhibited decreased UDS-TCR after irradiation (Fig. 5F). Lastly, we examined the effect of PARr-CSB expression on UDS-TCR after UV irradiation. We knocked down XPC from the earlier described U2OS CSB-ko cells that were rescued with the expression of CSB-wt or PARr-CSB

its N-terminal deletion fragments (pictogram) were reacted in vitro with purified PARP1 followed by PARP1-IP (left panel) or the *in vitro* PARylation assay (right panel). (**F, G**) CSB domains that accept PAR. (**F**) Top panel: PAR (10H)-IP pulled-down PARylated CSB and PARP1 from chromatin fraction of GM cells treated with Illudin S (30 ng/ml, 3 h). Bottom panels: Purified PARP1, CSB and control proteins GST and/or BSA were spotted on nitrocellulose membrane and reacted with free PAR followed by detection of PAR and the proteins. (**G**) Left panel: Purified PARP1, CSB, and its N-terminal deletion fragments [shown in panel (E) pictogram] and BSA were resolved on SDS–PAGE, blotted on membrane and reacted with free PAR followed by detection of PAR and proteins. Right panel: N-terminal domain of CSB is major PAR binding domain. HEK293 cells were transiently transfected with GFP tagged CSB and its nonoverlapping fragments [shown in panel (D) pictogram] for 48 h and subjected to GFP-IP followed by blotting on membrane and reaction with free PAR in SouthWestern assay followed by detection for PAR (10H) and GFP. # refers to nonspecific binding. (**H–J**) Mutations of key amino acids of PBM of CSB reduces the TCR and clonogenic survival after DNA damage**.** (**H**) The four Lys residues in the N-terminal PAR binding motif of CSB were mutated to Ala to create PAR-resistant—i.e. PARr-CSB (pictogram). The U2OS CSB-ko cells rescued with wild type CSB or PARr-CSB were exposed to UVC (30 J/m^2) and the chromatin extracts prepared after 1 h were subjected to RNAPIIS2-IP followed by detection of CSB and the downstream TCR proteins. The ratio of CSB/RNAPIIS2 was calculated for the immunoblot shown here, which is representative of three independent experiments. (**I**) The RRS was monitored for 18 h after UVC irradiation (10 J/m^2) in the indicated cell lines and expressed as RFI as described in Fig. 1 ($n = 2$). (**J**) Clonogenic survival after 24 h treatment with Illudin S for the indicated cell lines was expressed as mean ± SD ($n = 12$).

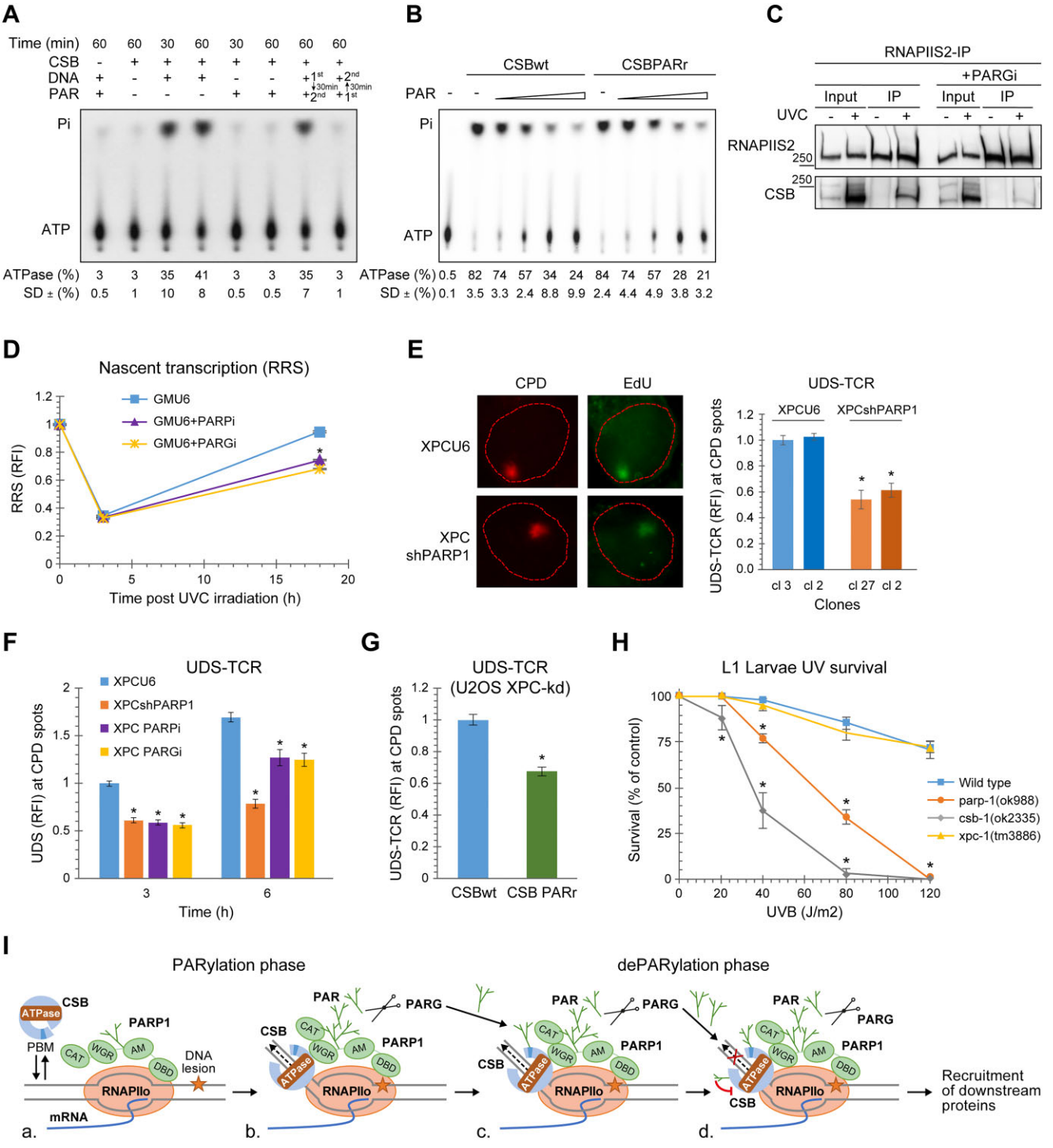

Figure 5. PAR suppresses ATPase activity of CSB and PARP1-depletion, inhibitors of PARP or PARG or N-terminal PAR-resistant CSB reduce TCR efficiency. (**A**) PAR abolishes the ATPase activity of CSB. The CSB was reacted individually or sequentially with 150 ng DNA and/or PAR, followed by quantification of the % of total ATP hydrolysed as Pi and expressed as mean ± SD ($n = 3$). (**B**) PAR dose-dependent inhibition of ATPase activity was identical for the wild type CSB and PARr-CSB. The purified CSB N-terminal PARr CSB and the wild-type form were reacted with 150 ng DNA and/or 15, 37.5, 75, and 150 ng PAR. The ATPase activity was quantified and presented, as described for above panel. (**C**) PARG inhibitor suppresses UVC (30 J/m^2)-induced interaction of CSB with RNAPII in the chromatin of GMU6 cells. (**D**) Identical suppression of RRS in GMU6 cells treated with PARPi or PARGi. Quantification of EU intensity in untreated or 3 and 18 h after 10 J/m^2 UV in GMU6 cells with or without PARPi or PARGi. Data derived from more than 100 nuclei from different fields and from two independent experiments are expressed as mean ± SE. Note that in all panels of this Fig., ∗ denotes statistically significant difference with unpaired two-tails *t*-test (*P*-value <.05). (**E**) PARP1-kd (shPARP1) clones in XP-C cells exhibit reduced TCR-specific UDS after local UVC irradiation (100 J/m^2). Local DNA damage identified by CPD staining. Data expressed as mean ± SE ($n = 3$). (**F**) As in panel (**E**), but also showing the effect PARPi or PARGi on the progression of UDS-TCR from 3 to 6 h. (**G**) The XPC-kd U2OS CSB-ko cells expressing wild type or PARr-CSB were locally irradiated to UVC (100 J/m^2) and monitored for UDS-TCR at 3 h. Data was expressed as mean ± SE from two independent experiments ($n = 200$–300 local irradiated spots). (**H**) Role of PARP1 in TCR is evolutionally conserved. Survival curve of *C. elegans* L1 larvae depleted for indicated genes in response to UVB. Data expressed as mean ± SE ($n = 3$). (**I**) Model for the roles of PARP1 and PARylation in stabilizing CSB with RNAPII in TCR.

(Supplementary Fig. S5J); and noted an impaired UDS-TCR capacity of PARr-CSB cells (Fig. 5G), which further confirmed that PARylation of N-terminal domain of CSB plays a key role in the progression of TCR. Collectively, these results reveal that PARP1 (shPARP1 model), PAR synthesis by PARP1 (PARPi model), PAR catabolism by PARG to release free PAR (PARGi model), PARylation of N-terminal domain of CSB (PARr-CSB model), and PARylation of C-terminal domain of CSB (ATPase assay with wt and PARr -CSB) contribute towards an efficient repair by TCR.

Loss of PARP1 reduces survival of TCR-dependent *C. elegans* L1 larvae to UV

Lastly, we examined the role of PARP1 in TCR in a whole organism by using *C. elegans* survival assays after exposure to UVB [59]. In nematodes, the resistance to UV is dependent on GGR in the germ cell and embryo state, whereas it depends on TCR in the L1 larvae stage of the worm. Using L1 larvae with loss of function mutations in *PARP1*, *CSB*, or *XPC* orthologs, we observed that while 75% of wild-type and GGR-deficient *XPC*-mutant larvae survived a 120 J/m^2 UVB irradiation, none of the *PARP1* or *CSB* mutant larvae survived at that dose (Fig. 5H). Thus, a significantly increased susceptibility to UV due to inefficient TCR in *PARP1*-mutant and the known TCR-deficient *CSB* mutant larvae, support an evolutionarily conserved role of PARP1 in TCR from worms to human cells.

Discussion

In mammalian cells, PARP1 is among the first responders to DNA damage with mechanistic roles in multiple DNA repair pathways, including GGR of UV-damaged DNA. Here, we describe a key early role for PARP1 and PARylation in significantly increasing the efficiency of TCR. We show that TCR is inefficient under the following circumstances: the absence of PARP1, inhibition of formation of PAR, inhibition of PARG-mediated degradation of PAR to form free PAR fragments that can noncovalently modify PAR-acceptor proteins, and the expression of CSB that is mutated at the PAR-acceptor sites in its N-terminal domain. Each of these circumstances independently decreased TCR at the earliest stage of stabilization of CSB with lesion stalled RNAPIIo that is required to initiate TCR. Lastly, in *C. elegans* L1 larvae, we identified PARP1 as a TCR-related gene, confirming an evolutionarily conserved role of PARP1 in TCR.

Based on our data and previous studies, we propose a model for the dual roles of PARP1 and PARylation in stabilization of CSB with the lesion stalled RNAPII to facilitate TCR (Fig. 5I, and Graphic summary). During normal transcription (step a), CSB dynamically probes but does not stably associate with the moving RNAPIIo that is transcribing the gene [54, 75]. For these normal housekeeping conditions, PARP1 associated with RNAPII would be basally stimulated to maintain low levels of PAR sufficient for its chromatin remodelling function, which is unlike the enhanced PARP1 activation and PARylation of specific proteins that occur at the DNA damage site [76]. When RNAPIIo stalls at the DNA lesion (step b), our co-IP and *in vitro* studies reveal that CSB interacts not only with RNAPII but also with PARP1. The interaction of different domains of PARP1 with CSB and RNAPII would result in the initial stabilization of all three proteins at the lesion site. The binding of CSB to DNA initiates its ATP-dependent lesion recognition by pulling the DNA (step b). Our model remains inclusive that CSA recruitment to the lesion site at this stage would further stimulate ATPase activity of CSB, as shown by Kokic *et al*. [77]. The CSB would increase the binding of PARP1 to damaged DNA and further stimulate its catalytic activity, resulting in additional auto-PARylation of PARP1. The accumulation of PAR recruits PARG resulting in the release of free PAR-fragments at the lesion site which would PARylate CSB (step c). The initial PARylation of CSB would occur preferentially at the N-terminal PBM of CSB, which has much higher affinity for PAR than its C-terminal domain. The N-terminal PAR-resistant CSB studies reveal that N-terminal PARylation of CSB further stabilizes the interaction of CSB with RNAPII, while still permitting the ATPase activity of CSB for lesion recognition. The continuing activity of PARG at the lesion site results in accumulation of free PAR in sufficient concentrations to bind to the C-terminal domain of CSB and completely suppress its ATPase activity (step d). Thus, PARP1 and PARG activity together at the lesion site define the short window of time for CSB to complete the lesion recognition step. This state permits CSB to maintain a stable interaction with RNAPII while being involved in the recruitment of downstream TCR proteins to lesion-arrested RNAPII.

Our results highlight similarities between the roles of PARP1 and PARylation in the initiation of both NER subpathways [78]. First of all, PARP1 interacts with two key proteins that act early in each sub-pathway: DBB2 and XPC in GGR; and CSB and RNAPII in TCR. Interestingly, in each case, PARP1 already stably interacts with one partner even in undamaged cells, which is XPC in GGR and RNAPII in TCR. Whereas, it interacts with the second partner, DDB2 in GGR and CSB in TCR, only after it has arrived independently from PARP1 at the DNA lesion site. The interaction of PARP1 with DDB2 or CSB stimulates its catalytic activity to form more PAR at the lesion site resulting in PARylation of these two partners, which facilitates the recruitment of downstream proteins for repair. The two step involvement of PARP1 with different partners further ensures that the repair is launched only when required. Interestingly, the absence of PARP1 or PARylation delays but not completely block the repair process by both GGR and TCR, yet the inefficient repair has long term consequence of decreased survival of the cells after DNA damage that is repaired by these two NER sub-pathways.

Our results add PARylation among other PTMs, such as ubiquitination, sumoylation, and phosphorylation that contribute significantly to facilitate and regulate TCR. The CSB binds to free PAR *in vitro* and in cells after Illudin S or UVC treatment (Fig. 4 and [71]). Mutating four Lysine residues to Alanine in the highly positively charged PBMs of CSB [30] abolishes its PAR-binding capacity at this site, reduces its interaction with RNAPII resulting in an inefficient TCR. Interestingly, these key Lys residues are conserved in higher organisms from chicken to humans, and their mutation has been shown to not influence the initial recruitment but to reduce the retention of CSB at the zone of local irradiation induced DNA damage [58]. This is an agreement with our results that although initial CSB recruitment to the chromatin fraction is PARP1 and PAR-independent, its interaction with RNAPII is facilitated by PAR binding to its N-terminal PAR binding motif. It will be interesting to examine whether PARylation and dePARylation of the multifunctional CSB could be broadly ex-

ploited in repair of different types of DNA damages in which CSB is known to be involved [51].

It is noteworthy that altering the cellular capacity for other PTMs [79], such as ubiquitination [80, 81], sumoylation [81, 82], and phosphorylation [83] also result in impaired TCR, despite having normal PARP1 and PARylation activities. For example, deleting the ubiquitin-binding domain does not reduce the initial interaction of CSB with stalled RNAPII, but it still decreases TCR and sensitizes the cells to UVC irradiation [80, 82]. Unlike other PTMs that are dependent on CSB at the lesion site, the role of PARP1 in TCR starts even before CSB arrives at the lesion site. Thus, our results strongly indicate that PARylation would be the earliest PTM to confer efficiency in TCR at the level of stabilization of CSB–RNAPII complex to launch TCR. In GGR, different PTMs have been shown to collaborate with or exhibit inter-dependence on each other [84]; therefore, it will be interesting to explore whether PARylation works collaboratively with other PTMs at the same or different steps of TCR to orchestrate an efficient repair.

Our results also highlight that PARylation is a flexible tool to control activity of ATPase function of various proteins. For example, PARylation upregulates ATPase function of chromatin remodeler ALC1 [85], but inhibits that of the nucleosome remodeling ISWI [86], as well as CSB as shown here. Earlier report by Thorsland *et al*. [71] revealed that PARylation of CSB blocks ATPase function. Our studies now clearly define that only the minor PARylation of C-terminal domain blocks ATPase, while major PARylation of CSB at N-terminal domain promotes the interaction of CSB with RNAPII. It has also been shown that deletion of 245-365 aa in CSB that includes the PARr mutation sites in our study, does not alter its ability to bind to chromatin or prevent DNA-stimulated ATPase function of CSB [21], which is in agreement with our results obtained with PARr-CSB model. In addition, our data shows that C-terminal PARylation by free PAR arising from the action of PARG requires a substantial build-up of PAR to completely suppress ATPase function of CSB. Thus, a significant difference in affinity for PAR by two ends of CSB and time required for PARG-mediated accumulation of free PAR together provide the window of time for lesion recognition step to be completed by CSB followed by shutdown of ATPase function which permits initiation of TCR. We suggest that if CSB is not degraded after its release form the lesion site, then its ATPase activity could be derepressed by eventually complete dePARylation of CSB permitting its recruitment to RNAPII stalled at other lesion sites.

Apart from PARylation, phosphorylation of CSB has also been shown to control ATPase activity of CSB. Christianssen *et al*. [87] demonstrated in an *in vitro* assay that CSB dephosphorylation stimulates its ATPase activity. However, they also showed that dephosphorylation of CSB takes several hours in cells. This also requires that CSB arrives at the lesion site in a phosphorylated and inactive ATPase state. In this respect, CSB was shown to be phosphorylated by casein kinase 2 in complex with ARK2N, but its impact on the ATPase activity of CSB was not examined [83] and the role of ARK2N in this process needs further clarification [88, 89]. Thus, phosphorylation-dephosphorylation is potentially a second mechanism for controlling the ATPase function of CSB for lesion recognition. However, this would require more studies to fully understand the kinetics and the state of phosphorylation and dephosphorylation of CSB before and after UV irradiation in the cells.

Our model remains inclusive for the discovery of additional roles of PARP1 and PARylation in facilitating downstream TCR events based on our Bio-ID proteomic profile and known PARylation of subsequent NER proteins, such as XPA [90] and DDB1 [40]. It will be interesting to verify whether PAR metabolism mediated transient control of ATPase activity of CSB is also implicated in other CSB-dependent DNA repair pathways; as well as in the ATPase activity of other proteins that are implicated in diverse responses to DNA damage apart from repair, such as chromatin remodelling. Finally, our results highlight the importance of timely and rapid completion of TCR, because even a partial suppression and a delay in this process, such as due to the absence of PARP1 and PAR metabolism, comes at a cost of increased sensitivity of the cell to a DNA damage that is repaired by TCR.

Acknowledgements

Author contributions: Mihaela Robu (Conceptualization [equal], Data curation [equal], Formal analysis [equal], Investigation [equal], Methodology [lead], Validation [equal], Visualization [equal], Writing—original draft [equal], Writing—review & editing [equal]); Rashmi G. Shah (Conceptualization [equal], Data curation [supporting], Formal analysis [supporting], Investigation [supporting], Methodology [supporting], Visualization [supporting], Writing—original draft [supporting], Writing—review & editing [supporting]; Diana van den Heuvel (Conceptualization [supporting], Data curation [supporting], Formal analysis [supporting], Methodology [supporting], Validation [supporting], Visualization [supporting], Writing—review & editing [supporting]); Yan Coulombe (Data curation [supporting], Formal analysis [supporting], Investigation [supporting], Methodology [supporting], Writing—review & editing [supporting]); Marc Bazin (Data curation [supporting], Methodology [supporting], Validation [supporting], Writing—review & editing [equal]); Melanie van der Woude (Data curation [supporting], Formal analysis [supporting], Investigation [supporting], Methodology [supporting], Validation [supporting], Writing—review & editing [supporting]); Angela Kragten (Data curation [supporting], Formal analysis [supporting], Investigation [supporting], Methodology [supporting], Validation [supporting]); Hannes Lans (Conceptualization [supporting], Data curation [supporting], Formal analysis [supporting], Funding acquisition [supporting], Investigation [supporting], Methodology [supporting], Project administration [supporting], Supervision [supporting], Validation [supporting], Visualization [supporting], Writing—review & editing [supporting]); John M. Pascal (Data curation [supporting], Formal analysis [supporting], Funding acquisition [supporting], Resources [supporting], Visualization [supporting], Writing—review & editing [supporting]); Jean-Yves Masson (Conceptualization [supporting], Data curation [supporting], Formal analysis [supporting], Funding acquisition [supporting], Investigation [supporting], Methodology [supporting], Supervision [supporting], Validation [supporting], Visualization [supporting], Writing—review & editing [supporting]); Martijn S. Luijsterburg (Conceptualization [supporting], Data curation [supporting], Formal analysis [supporting], Funding acquisition [supporting], Investigation [supporting], Methodology [supporting], Resources [supporting], Supervision [supporting], Validation [supporting], Visualization [supporting], Writing—original draft [supporting], Writing—review & edit-

ing [supporting]); Girish M. Shah (Conceptualization [lead], Data curation [equal], Formal analysis [equal], Funding acquisition [lead], Investigation [equal], Methodology [supporting], Project administration [Lead], Resources [lead], Supervision [lead], Validation [equal], Visualization [lead], Writing—original draft [lead], Writing—review & editing [lead])

Supplementary data

Supplementary data is available at NAR online.

Conflict of interest

None declared.

Funding

G.M.S. lab was supported by grants from NSERC Canada grants RGPIN-2016-05868, RGPIN-2022-05355, and FRQS grant to Research Centre of CHU de Quebec of Laval University. The open access publication was supported by the NSERC Canada grant RGPIN-2022-05355 to G.M.S. The J.M. lab was supported by Canadian Institutes of Health Research grant PJT374629. M.S.L. lab was supported by the Dutch Research Council (NWO) (VIDI grant ALW.016.161.320; VICI grant VI.C.212.005), and ERC Consolidator grant 101043815. J.Y.M. is a Canada Research Chair in DNA repair and cancer therapeutics, and was supported by CIHR project grant PGT-526991. H.L. lab was supported by Netherlands Organization for Scientific Research grant #711.018.007. Some *C. elegans* strains were provided by *C. elegans* Genetics Center.

Data availability

The data underlying this article will be shared on reasonable request to the corresponding author (girish.shah@crchul.ulaval.ca).

References

1. Nieto Moreno N, Olthof AM, Svejstrup JQ. Transcription-coupled nucleotide excision repair and the transcriptional response to UV-induced DNA damage. *Annu Rev Biochem* 2023;92:81–113. https://doi.org/10.1146/annurev-biochem-052621-091205
2. Mullenders LHF. Solar UV damage to cellular DNA: from mechanisms to biological effects. *Photochem Photobiol Sci* 2018;17:1842–52. https://doi.org/10.1039/c8pp00182k
3. Llerena Schiffmacher DA, Pai YJ, Pines A *et al.* Transcription-coupled repair: tangled up in convoluted repair. *FEBS J* 2025;292:5288–5323. https://doi.org/10.1111/febs.70104
4. Lu H, Yang M, Zhou Q. Reprogramming transcription after DNA damage: recognition, response, repair, and restart. *Trends Cell Biol* 2023;33:682–94. https://doi.org/10.1016/j.tcb.2022.11.010
5. Nakazawa Y, Hara Y, Oka Y *et al.* Ubiquitination of DNA damage-stalled RNAPII promotes transcription-coupled repair. *Cell* 2020;180:1228–1244 e1224. https://doi.org/10.1016/j.cell.2020.02.010
6. Jia N, Guo C, Nakazawa Y *et al.* Dealing with transcription-blocking DNA damage: repair mechanisms, RNA polymerase II processing and human disorders. *DNA Repair (Amst)* 2021;106:103192. https://doi.org/10.1016/j.dnarep.2021.103192
7. Schwertman P, Vermeulen W, Marteijn JA. UVSSA and USP7, a new couple in transcription-coupled DNA repair. *Chromosoma* 2013;122:275–84. https://doi.org/10.1007/s00412-013-0420-2
8. van der Weegen Y, de Lint K, van den Heuvel D *et al.* ELOF1 is a transcription-coupled DNA repair factor that directs RNA polymerase II ubiquitylation. *Nat Cell Biol* 2021;23:595–607. https://doi.org/10.1038/s41556-021-00688-9
9. Geijer ME, Zhou D, Selvam K *et al.* Elongation factor ELOF1 drives transcription-coupled repair and prevents genome instability. *Nat Cell Biol* 2021;23:608–19. https://doi.org/10.1038/s41556-021-00692-z
10. Kokic G, Yakoub G, van den Heuvel D *et al.* Structural basis for RNA polymerase II ubiquitylation and inactivation in transcription-coupled repair. *Nat Struct Mol Biol* 2024;31:536–47. https://doi.org/10.1038/s41594-023-01207-0
11. Ramadhin AR, Lee SH, Zhou D *et al.* STK19 drives transcription-coupled repair by stimulating repair complex stability, RNA Pol II ubiquitylation, and TFIIH recruitment. *Mol Cell* 2024;84:4740–4757. https://doi.org/10.1016/j.molcel.2024.10.030
12. Mevissen TET, Kummecke M, Schmid EW *et al.* STK19 positions TFIIH for cell-free transcription-coupled DNA repair. *Cell* 2024;187:7091–7106. https://doi.org/10.1016/j.cell.2024.10.020
13. van den Heuvel D, Rodriguez-Martinez M, van der Meer PJ *et al.* STK19 facilitates the clearance of lesion-stalled RNAPII during transcription-coupled DNA repair. *Cell* 2024;187:7107–7125. https://doi.org/10.1016/j.cell.2024.10.018
14. Tan Y, Gao M, Huang Y *et al.* STK19 is a transcription-coupled repair factor that participates in UVSSA ubiquitination and TFIIH loading. *Nucleic Acids Res* 2024;52:12767–83. https://doi.org/10.1093/nar/gkae787
15. Noe Gonzalez M, Blears D, Svejstrup JQ. Causes and consequences of RNA polymerase II stalling during transcript elongation. *Nat Rev Mol Cell Biol* 2021;22:3–21. https://doi.org/10.1038/s41580-020-00308-8
16. van der Meer PJ, Luijsterburg MS. The molecular basis of human transcription-coupled DNA repair. *Nat Cell Biol* 2025;27:1230–9. https://doi.org/10.1038/s41556-025-01715-9
17. van den Heuvel D, Spruijt CG, Gonzalez-Prieto R *et al.* A CSB-PAF1C axis restores processive transcription elongation after DNA damage repair. *Nat Commun* 2021;12:1342. https://doi.org/10.1038/s41467-021-21520-w
18. Tiwari V, Kulikowicz T, Wilson DM, 3rd *et al.* LEO1 is a partner for Cockayne syndrome protein B (CSB) in response to transcription-blocking DNA damage. *Nucleic Acids Res* 2021;49:6331–46. https://doi.org/10.1093/nar/gkab458
19. Wienholz F, Zhou D, Turkyilmaz Y *et al.* FACT subunit Spt16 controls UVSSA recruitment to lesion-stalled RNA Pol II and stimulates TC-NER. *Nucleic Acids Res* 2019;47:4011–25. https://doi.org/10.1093/nar/gkz055
20. Aydin OZ, Marteijn JA, Ribeiro-Silva C *et al.* Human ISWI complexes are targeted by SMARCA5 ATPase and SLIDE domains to help resolve lesion-stalled transcription. *Nucleic Acids Res* 2014;42:8473–85. https://doi.org/10.1093/nar/gku565
21. Cho I, Tsai PF, Lake RJ *et al.* ATP-dependent chromatin remodeling by Cockayne syndrome protein B and NAP1-like histone chaperones is required for efficient transcription-coupled DNA repair. *PLoS Genet* 2013;9:e1003407. https://doi.org/10.1371/journal.pgen.1003407
22. Llerena Schiffmacher DA, Lee SH, Kliza KW *et al.* The small CRL4(CSA) ubiquitin ligase component DDA1 regulates transcription-coupled repair dynamics. *Nat Commun* 2024;15:6374. https://doi.org/10.1038/s41467-024-50584-7
23. van Beek L, McClay E, Patel S *et al.* PARP power: a structural perspective on PARP1, PARP2, and PARP3 in DNA damage repair and nucleosome remodelling. *Int J Mol Sci* 2021;22:5112https://doi.org/10.3390/ijms22105112

24. Pascal JM. The comings and goings of PARP-1 in response to DNA damage. *DNA Repair (Amst)* 2018;71:177–82. https://doi.org/10.1016/j.dnarep.2018.08.022
25. Alemasova EE, Lavrik OI. Poly(ADP-ribosyl)ation by PARP1: reaction mechanism and regulatory proteins. *Nucleic Acids Res* 2019;47:3811–27. https://doi.org/10.1093/nar/gkz120
26. Dantuma NP, van Attikum H. Spatiotemporal regulation of posttranslational modifications in the DNA damage response. *EMBO J* 2016;35:6–23. https://doi.org/10.15252/embj.201592595
27. Pei J, Zhang J, Wang XD *et al.* Impact of Asp/Glu-ADP-ribosylation on protein-protein interaction and protein function. *Proteomics* 2023;23:e2200083. https://doi.org/10.1002/pmic.202200083
28. Pleschke JM, Kleczkowska HE, Strohm M *et al.* Poly(ADP-ribose) binds to specific domains in DNA checkpoint proteins. *J Biol Chem* 2000;275:40974–80. https://doi.org/10.1074/jbc.M006520200
29. Beneyton A, Nonfoux L, Gagne JP *et al.* The dynamic process of covalent and non-covalent PARylation in the maintenance of genome integrity: a focus on PARP inhibitors. *NAR Cancer* 2023;5:zcad043. https://doi.org/10.1093/narcan/zcad043
30. Gagne JP, Isabelle M, Lo KS *et al.* Proteome-wide identification of poly(ADP-ribose) binding proteins and poly(ADP-ribose)-associated protein complexes. *Nucleic Acids Res* 2008;36:6959–76. https://doi.org/10.1093/nar/gkn771
31. Brochu G, Duchaine C, Thibeault L *et al.* Mode of action of poly(ADP-ribose) glycohydrolase. *Biochim Biophys Acta* 1994;1219:342–50. https://doi.org/10.1016/0167-4781(94)90058-2
32. Pourfarjam Y, Kasson S, Tran L *et al.* PARG has a robust endo-glycohydrolase activity that releases protein-free poly(ADP-ribose) chains. *Biochem Biophys Res Commun* 2020;527:818–23. https://doi.org/10.1016/j.bbrc.2020.04.120
33. Suskiewicz MJ, Prokhorova E, Rack JGM *et al.* ADP-ribosylation from molecular mechanisms to therapeutic implications. *Cell* 2023;186:4475–95. https://doi.org/10.1016/j.cell.2023.08.030
34. Rouleau-Turcotte E, Pascal JM. ADP-ribose contributions to genome stability and PARP enzyme trapping on sites of DNA damage; paradigm shifts for a coming-of-age modification. *J Biol Chem* 2023;299:105397. https://doi.org/10.1016/j.jbc.2023.105397
35. Huang D, Kraus WL. The expanding universe of PARP1-mediated molecular and therapeutic mechanisms. *Mol Cell* 2022;82:2315–34https://doi.org/10.1016/j.molcel.2022.1002.1021
36. Azarm K, Smith S. Nuclear PARPs and genome integrity. *Genes Dev* 2020;34:285–301. https://doi.org/10.1101/gad.334730.119
37. Vodenicharov MD, Ghodgaonkar MM, Halappanavar SS *et al.* Mechanism of early biphasic activation of poly(ADP-ribose) polymerase-1 in response to ultraviolet B radiation. *J Cell Sci* 2005;118:589–99. https://doi.org/10.1242/jcs.01636
38. Pines A, Vrouwe MG, Marteijn JA *et al.* PARP1 promotes nucleotide excision repair through DDB2 stabilization and recruitment of ALC1. *J Cell Biol* 2012;199:235–49. https://doi.org/10.1083/jcb.201112132
39. Purohit NK, Robu M, Shah RG *et al.* Characterization of the interactions of PARP-1 with UV-damaged DNA *in vivo* and *in vitro*. *Sci Rep* 2016;6:19020. https://doi.org/10.1038/srep19020
40. Pines A, Mullenders LH, van Attikum H *et al.* Touching base with PARPs: moonlighting in the repair of UV lesions and double-strand breaks. *Trends Biochem Sci* 2013;38:321–30. https://doi.org/10.1016/j.tibs.2013.03.002
41. Robu M, Shah RG, Petitclerc N *et al.* Role of poly(ADP-ribose) polymerase-1 in the removal of UV-induced DNA lesions by nucleotide excision repair. *Proc Natl Acad Sci USA* 2013;110:1658–63. https://doi.org/10.1073/pnas.1209507110
42. Luijsterburg MS, Lindh M, Acs K *et al.* DDB2 promotes chromatin decondensation at UV-induced DNA damage. *J Cell Biol* 2012;197:267–81. https://doi.org/10.1083/jcb.201106074
43. Robu M, Shah RG, Purohit NK *et al.* Poly(ADP-ribose) polymerase 1 escorts XPC to UV-induced DNA lesions during nucleotide excision repair. *Proc Natl Acad Sci USA* 2017;114:E6847–56. https://doi.org/10.1073/pnas.1706981114
44. Blessing C, Apelt K, van den Heuvel D *et al.* XPC-PARP complexes engage the chromatin remodeler ALC1 to catalyze global genome DNA damage repair. *Nat Commun* 2022;13:4762. https://doi.org/10.1038/s41467-022-31820-4
45. Zong W, Gong Y, Sun W *et al.* PARP1: liaison of chromatin remodeling and transcription. *Cancers (Basel)* 2022;14:4162. https://doi.org/10.3390/cancers14174162
46. Krishnakumar R, Gamble MJ, Frizzell KM *et al.* Reciprocal binding of PARP-1 and histone H1 at promoters specifies transcriptional outcomes. *Science* 2008;319:819–21. https://doi.org/10.1126/science.1149250
47. Kotova EY, Hsieh FK, Chang HW *et al.* Human PARP1 facilitates transcription through a nucleosome and histone displacement by Pol II *in vitro*. *Int J Mol Sci* 2022;23:7107https://doi.org/10.3390/ijms23137107
48. Gibson BA, Zhang Y, Jiang H *et al.* Chemical genetic discovery of PARP targets reveals a role for PARP-1 in transcription elongation. *Science* 2016;353:45–50. https://doi.org/10.1126/science.aaf7865
49. Flohr C, Burkle A, Radicella JP *et al.* Poly(ADP-ribosyl)ation accelerates DNA repair in a pathway dependent on Cockayne syndrome B protein. *Nucleic Acids Res* 2003;31:5332–7. https://doi.org/10.1093/nar/gkg715
50. Ghodgaonkar MM, Zacal NJ, Kassam SN *et al.* Depletion of poly(ADP-ribose)polymerase-1 reduces host cell reactivation for UV-treated adenovirus in human dermal fibroblasts. *DNA Repair (Amst)* 2008;7:617–32. https://doi.org/10.1016/j.dnarep.2008.01.001
51. Bilkis R, Lake RJ, Fan HY. ATP-dependent chromatin remodeler CSB couples DNA repair pathways to transcription with implications for Cockayne syndrome and cancer therapy. *Cells* 2025;14:239https://doi.org/10.3390/cells14040239
52. Olivieri M, Cho T, Alvarez-Quilon A *et al.* A genetic map of the response to DNA damage in human cells. *Cell* 2020;182:481–496 e421. https://doi.org/10.1016/j.cell.2020.05.040
53. Shah RG, Ghodgaonkar MM, Affar EB *et al.* DNA vector-based RNAi approach for stable depletion of poly(ADP-ribose) polymerase-1. *Biochem Biophys Res Commun* 2005;331:167–74. https://doi.org/10.1016/j.bbrc.2005.03.135
54. van der Weegen Y, Golan-Berman H, Mevissen TET *et al.* The cooperative action of CSB, CSA, and UVSSA target TFIIH to DNA damage-stalled RNA polymerase II. *Nat Commun* 2020;11:2104. https://doi.org/10.1038/s41467-020-15903-8
55. Neveu B, Richer C, Cassart P *et al.* Identification of new ETV6 modulators through a high-throughput functional screening. *iScience* 2022;25:103858. https://doi.org/10.1016/j.isci.2022.103858
56. Steffen JD, McCauley MM, Pascal JM. Fluorescent sensors of PARP-1 structural dynamics and allosteric regulation in response to DNA damage. *Nucleic Acids Res* 2016;44:9771–83.
57. Kandan-Kulangara F, Shah RG, Affar EB *et al.* Persistence of different forms of transient RNAi during apoptosis in mammalian cells. *PLoS One* 2010;5:e12263. https://doi.org/10.1371/journal.pone.0012263
58. Scheibye-Knudsen M, Mitchell SJ, Fang EF *et al.* A high-fat diet and NAD(+) activate Sirt1 to rescue premature aging in Cockayne syndrome. *Cell Metab* 2014;20:840–55. https://doi.org/10.1016/j.cmet.2014.10.005
59. van der Woude M, Lans H. *C. elegans* survival assays to discern global and transcription-coupled nucleotide excision repair. *STAR Protoc* 2021;2:100586. https://doi.org/10.1016/j.xpro.2021.100586
60. Dubois ML, Bastin C, Levesque D *et al.* Comprehensive characterization of minichromosome maintenance complex (MCM) protein interactions using affinity

and proximity purifications coupled to mass spectrometry. *J Proteome Res* 2016;15:2924–34. https://doi.org/10.1021/acs.jproteome.5b01081
61. Batenburg NL, Mersaoui SY, Walker JR *et al.* Cockayne syndrome group B protein regulates fork restart, fork progression and MRE11-dependent fork degradation in BRCA1/2-deficient cells. *Nucleic Acids Res* 2021;49:12836–54. https://doi.org/10.1093/nar/gkab1173
62. Langelier MF, Planck JL, Servent KM *et al.* Purification of human PARP-1 and PARP-1 domains from Escherichia coli for structural and biochemical analysis. *Methods Mol Biol* 2011;780:209–26.
63. Shah GM, Kandan-Kulangara F, Montoni A *et al.* In: Tulin A. V. (ed.), *Methods in Molecular Biology: "Poly(ADP-ribose) Polymerase: Methods and Protocols"*. First ed. Springer New York, NY, USA: Humana Press, 2011, Vol. 780, 3–34.
64. Jaspers NG, Raams A, Kelner MJ *et al.* Anti-tumour compounds illudin S and Irofulven induce DNA lesions ignored by global repair and exclusively processed by transcription- and replication-coupled repair pathways. *DNA Repair (Amst)* 2002;1:1027–38. https://doi.org/10.1016/S1568-7864(02)00166-0
65. Schwertman P, Lagarou A, Dekkers DH *et al.* UV-sensitive syndrome protein UVSSA recruits USP7 to regulate transcription-coupled repair. *Nat Genet* 2012;44:598–602. https://doi.org/10.1038/ng.2230
66. Jia N, Nakazawa Y, Guo C *et al.* A rapid, comprehensive system for assaying DNA repair activity and cytotoxic effects of DNA-damaging reagents. *Nat Protoc* 2015;10:12–24. https://doi.org/10.1038/nprot.2014.194
67. Geijer ME, Marteijn JA. What happens at the lesion does not stay at the lesion: transcription-coupled nucleotide excision repair and the effects of DNA damage on transcription in cis and trans. *DNA Repair (Amst)* 2018;71:56–68. https://doi.org/10.1016/j.dnarep.2018.08.007
68. Mayne LV, Lehmann AR. Failure of RNA synthesis to recover after UV irradiation: an early defect in cells from individuals with Cockayne's syndrome and xeroderma pigmentosum. *Cancer Res* 1982;42:1473–8.
69. Chen FX, Smith ER, Shilatifard A. Born to run: control of transcription elongation by RNA polymerase II. *Nat Rev Mol Cell Biol* 2018;19:464–78. https://doi.org/10.1038/s41580-018-0010-5
70. Dawicki-McKenna JM, Langelier MF, DeNizio JE *et al.* PARP-1 activation requires local unfolding of an autoinhibitory domain. *Mol Cell* 2015;60:755–68. https://doi.org/10.1016/j.molcel.2015.10.013
71. Thorslund T, von Kobbe C, Harrigan JA *et al.* Cooperation of the cockayne syndrome group B protein and poly(ADP-ribose) polymerase 1 in the response to oxidative stress. *Mol Cell Biol* 2005;25:7625–36. https://doi.org/10.1128/MCB.25.17.7625-7636.2005
72. Mourgues S, Gautier V, Lagarou A *et al.* ELL, a novel TFIIH partner, is involved in transcription restart after DNA repair. *Proc Natl Acad Sci USA* 2013;110:17927–32. https://doi.org/10.1073/pnas.1305009110
73. Robu M, Shah RG, Shah GM. Methods to study intracellular movement and localization of the nucleotide excision repair proteins at the DNA lesions in mammalian cells. *Front Cell Dev Biol* 2020;8:590242. https://doi.org/10.3389/fcell.2020.590242
74. Limsirichaikul S, Niimi A, Fawcett H *et al.* A rapid non-radioactive technique for measurement of repair synthesis in primary human fibroblasts by incorporation of ethynyl deoxyuridine (EdU). *Nucleic Acids Res* 2009;37:e31. https://doi.org/10.1093/nar/gkp023
75. van den Boom V, Citterio E, Hoogstraten D *et al.* DNA damage stabilizes interaction of CSB with the transcription elongation machinery. *J Cell Biol* 2004;166:27–36. https://doi.org/10.1083/jcb.200401056
76. Thomas C, Ji Y, Wu C *et al.* Hit and run versus long-term activation of PARP-1 by its different domains fine-tunes nuclear processes. *Proc Natl Acad Sci USA* 2019;116:9941–6. https://doi.org/10.1073/pnas.1901183116
77. Kokic G, Wagner FR, Chernev A *et al.* Structural basis of human transcription-DNA repair coupling. *Nature* 2021;598:368–72. https://doi.org/10.1038/s41586-021-03906-4
78. Apelt K, Lans H, Scharer OD *et al.* Nucleotide excision repair leaves a mark on chromatin: DNA damage detection in nucleosomes. *Cell Mol Life Sci* 2021;78:7925–42. https://doi.org/10.1007/s00018-021-03984-7
79. Spyropoulou Z, Papaspyropoulos A, Lagopati N *et al.* Cockayne Syndrome Group B (CSB): the regulatory framework governing the multifunctional protein and its plausible role in cancer. *Cells* 2021;10:866. https://doi.org/10.3390/cells10040866
80. Anindya R, Mari PO, Kristensen U *et al.* A ubiquitin-binding domain in Cockayne syndrome B required for transcription-coupled nucleotide excision repair. *Mol Cell* 2010;38:637–48. https://doi.org/10.1016/j.molcel.2010.04.017
81. Liebelt F, Schimmel J, Verlaan-de Vries M *et al.* Transcription-coupled nucleotide excision repair is coordinated by ubiquitin and SUMO in response to ultraviolet irradiation. *Nucleic Acids Res* 2020;48:231–48.
82. Sin Y, Tanaka K, Saijo M. The C-terminal region and SUMOylation of Cockayne syndrome group B protein play critical roles in transcription-coupled nucleotide excision repair. *J Biol Chem* 2016;291:1387–97. https://doi.org/10.1074/jbc.M115.683235
83. Luo Y, Li J, Li X *et al.* The ARK2N-CK2 complex initiates transcription-coupled repair through enhancing the interaction of CSB with lesion-stalled RNAPII. *Proc Natl Acad Sci USA* 2024;121:e2404383121. https://doi.org/10.1073/pnas.2404383121
84. Van Houten B, Schnable B, Kumar N. Chaperones for dancing on chromatin: role of post-translational modifications in dynamic damage detection hand-offs during nucleotide excision repair. *Bioessays* 2021;43:e2100011. https://doi.org/10.1002/bies.202100011
85. Ahel D, Horejsi Z, Wiechens N *et al.* Poly(ADP-ribose)-dependent regulation of DNA repair by the chromatin remodeling enzyme ALC1. *Science* 2009;325:1240–3. https://doi.org/10.1126/science.1177321
86. Sala A, La Rocca G, Burgio G *et al.* The nucleosome-remodeling ATPase ISWI is regulated by poly-ADP-ribosylation. *PLoS Biol* 2008;6:e252. https://doi.org/10.1371/journal.pbio.0060252
87. Christiansen M, Stevnsner T, Modin C *et al.* Functional consequences of mutations in the conserved SF2 motifs and post-translational phosphorylation of the CSB protein. *Nucleic Acids Res* 2003;31:963–73. https://doi.org/10.1093/nar/gkg164
88. van Schie JJM, Brussee SJ, Luijsterburg MS. Evidence that ARK2N is not a core factor in transcription-coupled DNA repair. *Proc Natl Acad Sci USA* 2025;122:e2425178122. https://doi.org/10.1073/pnas.2425178122
89. Luo Y, Li J, Wang J. Reply to van Schie et al.: ARK2N in TCR: across *in vivo* and *in vitro* studies. *Proc Natl Acad Sci USA* 2025;122:e2426163122. https://doi.org/10.1073/pnas.2426163122
90. Fischer JM, Popp O, Gebhard D *et al.* Poly(ADP-ribose)-mediated interplay of XPA and PARP1 leads to reciprocal regulation of protein function. *FEBS J* 2014;281:3625–41. https://doi.org/10.1111/febs.12885

Received: January 31, 2025. **Revised:** October 22, 2025. **Accepted:** October 23, 2025